Quaternary Science Reviews 330 (2024) 108451

Contents lists available at ScienceDirect

Quaternary Science Reviews

journal homepage: www.elsevier.com/locate/quascirev

Chronology of Pleistocene sedimentary cycles in the western Mediterranean

Laura del Valle [a,b,c,*], Alida Timar-Gabor [a,b], Joan J. Fornós [c]

[a] Institute for Interdisciplinary Research in Bio-Nano-Sciences, Babeş-Bolyai University, Treboniu Laurian 42, 400271, Cluj-Napoca, Romania
[b] Faculty of Environmental Sciences and Engineering, Babeş-Bolyai University, Fântânele 30, 400327, Cluj-Napoca, Romania
[c] Earth Science Research Group, Faculty of Sciences, University of the Balearic Islands, Ctra. de Valldemossa, km 7.5, 07122, Palma (Mallorca), Spain

ARTICLE INFO

Handling editor: A. Voelker

Keywords:
Pleistocene
Holocene
OSL
Climatic change
Landscape evolution

ABSTRACT

This study focuses on the sedimentological and stratigraphic description and chronology of Pleistocene coastal deposits on the Pityusic Islands (Balearic Islands, Spain). These deposits show evidence of interference between processes characteristic of alluvial, marine, and aeolian environments. Optically stimulated luminescence dating of aeolian levels indicates that deposition took place from the Lower to Upper Pleistocene. The sedimentological and chronological analysis of these deposits allows reconstruction of coastal Pleistocene environmental history from MIS 22 to MIS 2. The results show that changes in the average wind direction over time, modulated by the interaction with coastal relief orientation, were the main controls on the Lower to Upper Pleistocene coastal landscape evolution on the Pityusic Islands. The main episodes of aeolian activity identified in the Western Mediterranean, can be linked to periods of low sea level. The study's findings the presence of two dominant environments, coastal aeolian and alluvial, each characterized by distinct geological processes. Interestingly, these processes have led to the formation of deposits that exhibit a combination of characteristics from both environments. Moreover, these deposits retain elements inherited from each environment in terms of sedimentary supply, precipitation, runoff or aeolian transport. These results corroborated by OSL dating provide a useful indicator of the geomorphological processes and changes that occurred during the Pleistocene, unraveling the environmental evolution, and contributing to the growing knowledge on western Mediterranean aeolian or aeolian-alluvial interacting environments during the last 1000 ka.

1. Introduction

The Pleistocene epoch, which lasted from 2.6 million to 11,700 years ago, was characterized by significant climatic fluctuations and landscape changes. The western Mediterranean region was no exception and experienced profound alterations in its natural environment during this time. Therefore, the Pleistocene epoch was a time of great environmental change, marked by repeated cycles of glacial and interglacial intervals. These changes had a significant impact on the sedimentation patterns of the western Mediterranean region. The chronology of these sedimentary cycles provides valuable insights into the evolution of the region's landscape, climate, and biota during the Pleistocene. The study of the chronology of Pleistocene sedimentary cycles in the Western Mediterranean is crucial for understanding the environmental changes that have shaped the region over time. In this sense, the study of the Pleistocene deposits of the Pityusic Islands (Eivissa, Formentera and Es Freus) can provide a valuable source of information for gaining a better understanding of the history of the climate and environmental conditions, as well as the geomorphological processes that occurred during the Quaternary. Pleistocene coastal deposits, such as aeolianites, colluvial-alluvial deposits, marine deposits, or palaeosols preserved along mid-latitude coastlines, are used to unravel the sedimentary response of shifting shorelines to sea level change (e.g., Porat and Botha, 2008; Bateman et al., 2011). When dated precisely, these deposists can provide paleoclimatic records of regional and global significance (El-Asmar, 1994; Kindler and Hearty, 1995, 1996; Clemmensen et al., 1997; Kindler et al., 1997; Hearty, 1998; Kocurek, 1998; Mauz, 1999; Rose et al., 1999; Sun et al., 1999; Blay and Longman, 2001; Brooke, 2001; Clemmensen et al., 2001; del Valle et al, 2016; Fornós et al., 2009; Pomar et al., 2018; Roberts et al., 2012). This research will help us better understand the complex interplay between the region's geological, climatic, and biotic systems, and how they have interacted to shape the Western Mediterranean landscape as we know it today.

* Corresponding author. Institute for Interdisciplinary Research in Bio-Nano-Sciences, Babeş-Bolyai University, Treboniu Laurian 42, 400271, Cluj-Napoca, Romania.
E-mail address: laura.del-valle@uib.eu (L. del Valle).

https://doi.org/10.1016/j.quascirev.2023.108451
Received 27 September 2023; Received in revised form 29 November 2023; Accepted 29 November 2023
Available online 14 March 2024

2. Sites and geological setting

This study presents data from seventeen Pleistocene deposit sites across Pityusic Islands (Eivissa, Formentera and Es Freus) (see Fig. 1). The paper includes new data obtained from three sites: Illa des Penjats, Illa des Porcs and Illa d'es Caragol in Es Freus; Punta Rasa and Cala Savina in Formentera, and Portitxol and Cap Martinet in Eivissa. To provide an overview of Pleistocene deposits in the western Mediterranean region, the presentation and discussion of the data from these sites are combined with data from other recently published sites, including the western coast of Eivissa (Anechitei-Deacu et al., 2018; **del Valle et al., 2020a**), Cala Xuclar in the northern coast of Eivissa (**del Valle et al., 2016**), S'estanyol and Es Codolar in the south coast of Eivissa (**del Valle, 2016**), S'Espalmador (**del Valle et al., 2019**), Cala en Baster in Formentera (del Valle et al., 2020b) and Es Ram- Es Copinar Formentera (**Bardají et al., 2017**; **del Valle et al., 2021a**) (Fig. 1C).

2.1. Geological settings

Shallow marine to continental Pleistocene deposits are continuously exposed along the coast of the Pityusic Islands, which is tectonically stable region (**Sàbat et al., 2011**; **Just et al., 2011**). The Pityusic Islands consist of two large islands, Eivissa and Formentera, and sixty islets, which are the emerged part of the southern block of the Balearic Promontory (**see** Fig. 1B) located in the westernmost part of the Mediterranean. The Es Freus islets are separated from Formentera by a narrow and shallow passage (50 m wide, −2 m deep). The lithology of Eivissa mainly consists of folded Jurassic limestones, Cretaceous marlstones, and Miocene marlstones, while Formentera is mainly composed of Miocene and Quaternary calcarenite and limestone deposits (**García de Domingo et al., 2009**). The Quaternary deposits, in both islands, overlie the Jurassic, Cretaceous and Miocene deposits, infilling the valleys and central depressions of the islands, and cover most of the coastal sections. The Es Freus islets are entirely composed of Quaternary dune fields (aeolianites), silty-sandy palaeosoils with calcrete crusts, partially covered by Holocene dunes. The basement only crops out in the Espalmador Islet and is formed by conglomerates belonging to the Miocene, which is a continuation of Formentera's basement.

All the sectors are characterized by thick aeolian deposits interbedded with colluvial deposits and palaeosoils. The Pleistocene sequences are delimited by an unconformity overlying the lower Miocene basement, which is made up of ancient alluvial fan conglomerates or massive lower Jurassic dolomites. The sedimentary successions containing Pleistocene coastal aeolianites at the Pityusic Islands display a wide variety of deposits characterized by colluvial facies and palaeosoils and some shallow marine facies interbedded. The rugged geomorphology of the coasts and the basement palaeotopography contributes to the complex architecture of these deposits (**Pomar et al., 2015**; **del Valle et al., 2016**).

3. Methods and instrumentation

We used the conventional method of lithostratigraphic logging as described by **Tucker (1988)**. Supplementary data on cross-bed dip direction for paleocurrent analyses were acquired, and grain size and mineralogy analyses were carried out.

We measured 213 stratigraphic logs (as shown in Fig. 2), interpreted and correlated based on major unconformities and homogeneous units, bounding surfaces, or according to the presence of continuous pedogenetic deposits. Major changes in facies vertically and laterally were considered. Each log's major units were characterized in terms of grain size, composition, and mineralogy, as well as its arrangement or architecture and facies associations (geometry and sedimentary bodies). We collected both marine and continental fossil macrofauna for taxonomic identification (**World Register of Marine Species** **WoRMS, 2020**), wherever possible.

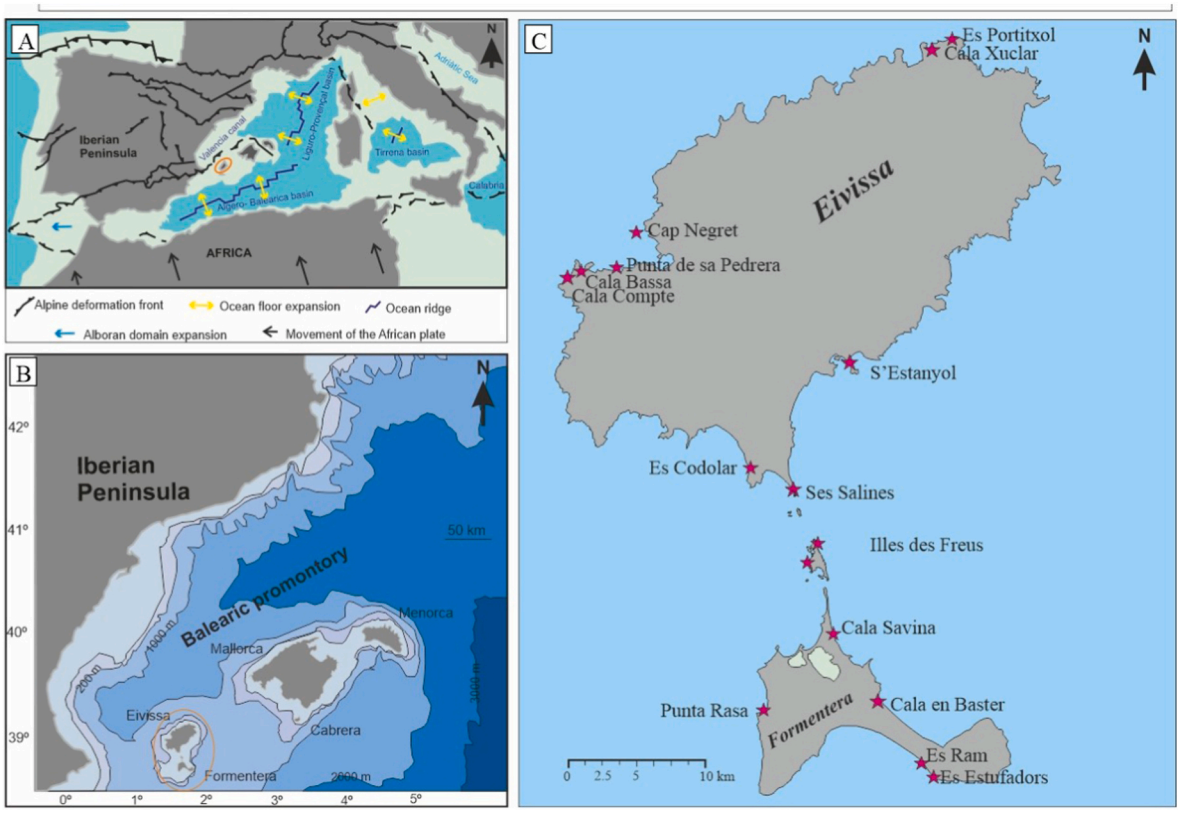

Fig. 1. Location of the study areas. A) Tectonic setting (Modified from Díaz, 2009); B) Location of Pityusic Islands (orange circle) within the Balearic Archipelago; G) Location of the study areas (purple stars).

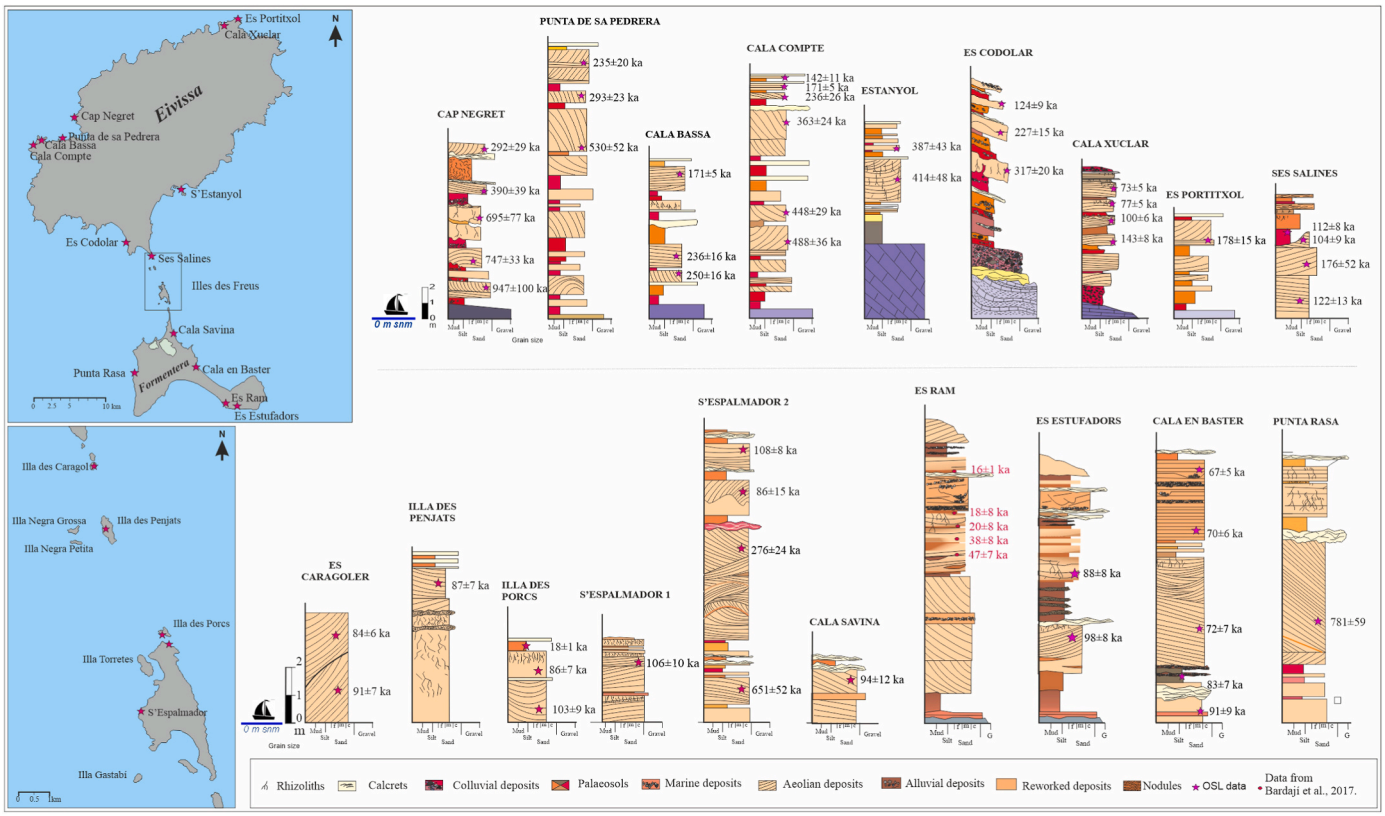

Fig. 2. Synthetic stratigraphic logs, location and OSL data from all the study areas.

The mineralogical content was determined using a Brucker D8-Advance X-ray diffractometer, using randomly oriented powders of the bulk samples that had been pre-treated with H_2O_2 to remove organic matter. The pressed powder diffraction patterns were recorded from 3° to 65° 2θ in steps of 0.03° with a 0.3 s counting time per step, at 25 °C room temperature, and logged to data files for analysis. Semi-quantitative mineral analyses were based on the peak areas obtained using Difracc EVA v.4.1 software.

We determined the colours by comparing sediment samples with the **Munsell Color Table, Soil Color Chart (2000),** and assigned the most similar reference code.

The sediment composition analysis was performed by point counting 250 to 500 grains from each grain size fraction under a binocular microscope using the count and composition plate of ***SedimPlak* (P202130758)**. Grains were classified into three classes, including lithoclasts, bioclasts and others. For the grain size analysis, one face of each sample was cut to create a flat surface, and the samples were washed with a solution of hydrochloric acid reduced to 10% to enhance the grain boundary. These pieces were studied under an optical microscope (NATIONAL Digital Microscope) which, along with the MoticImages Plus 2.0 image analysis software and the ImagJ.ink digital image analysis software, allowed the measurement of grain size parameters by sampling 20 grains per photo and calculating the average of the major axis.

3.1. Luminescence dating

3.1.1. Sample collection and preparation

A total of fifty-one samples were collected for optically stimulated luminescence (OSL) dating, of which fourteen are new to this paper. The samples were extracted from stratigraphic layers considered to be representative of the sequences at Cap Negret (5 samples), Punta de sa Pedrera (3 samples), Cala Bassa (3 samples), Cala Compte (4 samples); S'Estanyol (2 samples) (del Valle, 2016; del Valle et al., 2020a); Cala Xuclar (4 samples) (del Valle et al., 2016); Es Ram (2 samples) (del Valle et al., 2021a); Es Codolar (3 samples) (del Valle et al., 2021b); Cala en Baster (5 samples) (del Valle et al., 2020b) Ses Salines (4 samples) (del Valle et al., 2020c), Espalmador (5 samples); Portitxol (1 sample); Illa des Penjats (1 sample); Illa des Porcs (3 samples); Illa Caragol (2 samples); Cala Savina (1 sample); Punta Rasa (1 sample). Samples were detached under low light conditions, wrapped in light-proof material, labelled, and documented.

In order to extract siliciclastic grains, primarily quartz, the inner part of each sample was extracted in the laboratory to ensure that the material was not exposed to sunlight. The samples were repeatedly treated with hydrochloric acid (HCl) (35%) to remove calcium carbonate, followed by treatment with hydrogen peroxide treatment (H_2O_2) (30%) to remove organic matter. Coarse grain fractions (>63 μm) were separated through dry sieving. To isolate the quartz from the plagioclase feldspars and other minerals, a treatment with 40% hydrofluoric acid (HF) was performed. This HF etching also removed the outer surface of the quartz grains, reducing the external ionizing alpha radiation contribution to the grains to a negligible level. Precipitated fluorides resulted after HF attack and were washed away with a 60-min treatment in 10% HCl.

Luminescence measurements were performed using a TL/OSL Risø DA-20 readers, equipped with an automated detection and stimulation head (DASH) (**Lapp et al., 2015**). Luminescence signals were detected by a PDM 9107Q-AP-TTL-03 photomultiplier. A 7.5 mm thick Hoya U-340 UV filters were used for the detection of the quartz signals. Irradiation of the samples was completed using the incorporated ^{90}Sr–^{90}Y beta source, calibrated using gamma irradiated calibration quartz (**Hansen et al., 2015**). Dose rates of 0.149, 0.0943 and 0.0938 Gy/s were derived for the coarse quartz grains deposited on stainless steel disks, at the moment of measurement. Luminescence investigations were carried out using the single-aliquot regenerative dose (SAR) protocol (**Murray and Wintle, 2000, 2003**). Continuous wave stimulation of the luminescence signals with the blue light emitting diodes was performed for 40 s at 125 °C. The net CW-OSL signal was evaluated from

the first 0.308 s of the decay curve with an early background subtraction assessed from the 1.69–2.30 s interval. A preheat temperature of 220 °C for 10 s and a cut heat to 180 °C were employed throughout the SAR protocol. The OSL response to a fixed test dose of 16 Gy was used through the whole set of measurements to correct for sensitivity changes.

At the end of each SAR cycle a high-temperature bleach for 40 s at 280 °C was performed by stimulation with the blue diodes (Murray and Wintle, 2003). The purity of the signal from the extracted quartz was evaluated using the infrared stimulated luminescence (IRSL) response at 60 °C to a regenerative β-dose. A significant sensitivity to infrared stimulation accounts for an IR depletion ratio deviating more than 10% from unity (Duller, 2003). Radionuclide (Ra-226 and daughters, assumed in equilibrium with ^{238}U, ^{232}Th and daughters, ^{40}K) specific activities for annual dose estimation in luminescence dating were measured by high-resolution gamma spectrometry. Dose rates were derived based on the conversion factors tabulated by Adamiec and Aitken (1998).

For the age estimation the beta attenuation and etching factor considered for 63–250 μm fraction was 0.900 ± 0.060 and also an internal dose rate of 0.01 ± 0.002 Gy/ka (Vandenberghe et al., 2008). The cosmic ray component of the dose rate was calculated using the equations published by Prescott and Hutton (1994). A water content value of 3% by weight (with a relative error of 25%) was considered for moisture correction in age calculation. This relative average moisture value is similar to the values previously reported for other aeolianite samples from this area (i.e. Fornós et al., 2009; del Valle et al., 2016).

4. Results

4.1. Sedimentary facies and palaeosoil description

The sedimentology and stratigraphic analyses performed have allowed for the identification of three major facies associations and different types of palaeosoils (see Fig. 3).

4.1.1. Aeolian facies association

This facies is characterised by white colour in the upper levels to very

Fig. 3. Main characteristics of the sedimentary facies and their interpretation in terms of depositional processes. Facies are labelled using the following nomenclature C: conglomerate, B: breccia; S: sandstone and P: palaeosoil), dominant texture (a: sand, m: mud, s: silt), grain size (c: cobble, d: pebbles, e: medium to very coarse sand; h: fine to medium sand), sedimentary structures (l: laminated, p: planar cross-bedded, t: through cross-bedded, u: low angle cross-bedded, g: sorting), biogenic features (f: highly fossiliferous, r: root-races).

pale brown in the lower levels. It is comprised of well-sorted, fine to medium-grained bioclastic sand (125–250 μm) with trough cross-stratified beds that laterally decrease in angle from 30° to 10°. Beds are 0.7–3 m thick, and in the majority of cases, the upper part of these levels is partially disrupted by vertical root casts (1–6.5 cm width and 0.20–1 m length). The average grain composition is mainly carbonate (94%) composed of marine bioclasts with very little terrigenous material. Semi-quantitative data obtained by means of X-Ray diffraction analysis, the upper aeolian levels show a high percentage of aragonite (~51%) and calcite (~48%), followed by dolomite (5–20%). For the lower aeolian levels, the predominant mineral is calcite with an average of 93–99% (Table 1).

4.1.2. Colluvial-alluvial facies association

Two levels have been described. The first is characterized by reddish, silty, matrix-supported breccia with angular and heterometric clasts forming layers of deposits that are millimetre to centimetre thick, which are disrupted by calcretes levels. Some breccia layers change laterally into lens-shaped structures. The abundant subangular clasts originate from the reworked upper surface of the lower level. The mineralogical composition of the matrix is dominated by silicates (60%). These facies are interpreted as hillslope deposits.

The second level is formed by subangular cobble-sized sandstone filling ribbon-like channel incisions in aeolian deposits. No specific clast orientation is observed. The matrix-supported sandstone is composed of bioclastic sands with a fine to medium grain size. The mineralogical composition is dominated by calcite (53.9%) and aragonite (46.1%). This facies is interpreted as intraformational sandstone-conglomerate channel fill.

4.1.3. Shallow marine facies association

This facies is characterized by massive strata (with a maximum thickness of around 40 cm) with subrounded/rounded clasts mostly in discoidal form and interstices filled by medium to coarse grained sand rich in bioclasts and entire marine macrofossils. The colour is very pale brown. The mineralogical composition is dominated by calcite (55%)

Table 1
Mineral content of the samples.

	Sample code	Calcite (%)	Aragonite (%)	Dolomite (%)	Brushite (%)	Quartz (%)	Orthoclase (%)	Unidentified (%)
Cala Bassa	M#11#	75.9	-	10.6	-	7.6	-	5.8
	M#9#	88.4	-	4.2	-	2	1.6	3.8
	M#6#	67.1	-	10.5	-	13.6	1.2	7.7
Cala Compte	M#15#	74	-	11	-	5	2	8
	M#16#	81.2	-	5.3	-	5.2	1.1	7.2
	M#17#	76.5	3.7	10	-	8.2	-	1.59999999999999
	M#20#	72	11	12	-	5	-	-
Cap Negret	M#27#	99.9	-	-	-	0.1	-	-
	M#26#	96.6	-	-	-	3.4	-	-
	M#36#	94	-	1.3	-	4.7	-	-
	M#33#	88	-	2	-	6.5	-	3.5
	M#2#	74.6	4.2	10.5	-	5.1	1.9	3.7
	M#3#	79	3.4	7.2	-	5.8	2.6	2
Punta de sa Pedrera	M#5#	80	-	5.3	-	10	1.5	3.2
	M#4#	77	-	16	-	1.2	-	5.8
	M#49#	88.6	-	1.5	-	3.8	-	6.09999999999999
ES Ram	M#ES2#	45.6	48.3	6.1	-	-	-	-
	M#ES7#	58.9	30.8	8.8	-	1.5	-	-
Cala Xuclar profile	M#D1#	85	-	5	-	1	-	-
	M#D2#	66	4	10	-	6	-	-
	M#D3#	70	8	12	-	3.4	-	-
	M#D4#	42.1	23.5	14.5	-	4	-	-
S'Estanyol profile	M#60#	82	-	12.3	-	10	-	-
	M#63#	80	-	15.2	-	8	-	-
Es Codolar profile	M#22#	72	-	9	-	0.6	-	-
	M#24#	80	-	7.8	-	1.8	-	-
	M#26#	82	-	10.3	-	-	-	-
	Pmn	33	-	-	-	39.1	2.5	9
	Par	75	-	-	-	12	7	-
ses Salines	#SS2#	60	40	-	-	-	-	-
	#SS1#	48.7	51.3	-	-	-	-	-
	#SS0#	62.8	37.2		-			
Espalmador profile	#MEO#	49.3	50.7	-	-	-	-	-
	#ME1#	95.7	-	2.5	-	2.5	-	-
	#ME2#	86.7	-	11.4	-	1.9	-	-
	#ME3#	71.6	11.9	15.2	-	1.2	-	-
	#ME4#	69.7	20.7	5.2	-	4.4	-	-
Cala en Baster profile	#CB1#	40.8	51.6	7.6	-	-	-	-
	#CB3#	43.2	22.6	33.2	-	1	-	-
	#CB4#	63.9	29.4	4.9	-	1.8	-	-
	#CB5#	67.5	25.5	4	-	3	-	-
Illa d'es Penjats profile	#IP2#	57.3	42.7	-	-	-	-	-
Illa d'es Porcs profile	#IPC3#				-			
	#IPC1#	58	26	11	-	2.1	-	-
	#IPC2#	42	51	7	-	0.3	-	-
Illa d'es Caragol profile	#IC1#	42.5	49	8.5	-	-	-	-
	#IC2#	21.3	35.3	23.5	19.9	-	-	-
Cala Sabina profile	#CS1#	53.9	46.1	-	-	-	-	-
Es Portitxol profile	#MP1#	75.1	17.8	5	-	2.2	-	-
Punta Rasa profile	#MF1#	99.4	-	-	-	0.6	-	-

and aragonite (45%).

4.1.4. Palaeosoils

In general terms, two types of palaeosoils are observed. The first type is characterized by massive silty-sandy texture that is highly bioturbated by vegetation. Its colour is very pale brown, and it bears abundant terrestrial fauna (e.g. the endemic land snail *Xerocrassa ebusitana* and insect trace fossils). This sandy palaeosoil shows variable thickness, changing laterally from 0.5 m to 1.5 m. In general, in the upper part, 5 cm thick calcretes are observed capping the palaeosoil. The composition of the silts and sands is mainly carbonate (~80%) with calcite as the major mineral (57%), followed by the aragonite with 23% and minor amounts of quartz (2%).

The second type of palaeosoils are characterized by the presence of reddish to yellow clays and silts and showing with iron bands. The mineralogical content shows 56% clay minerals, of which illite clays makes up 40%, 20% quartz, and a minor content of calcite (11%). Calcretes have been observed locally with pisoliths horizons and abundant vegetal traces. These calcretes show calcified branched filamentous structures. The red mudstone palaeosoil levels show variable thickness, changing laterally from 0.10 m to 0.5 m.

4.2. OSL ages and performance of the measurement protocol

As previously reported for this region (**Anechitei-Deacu et al., 2018**) the quartz from the aeolianites from the Pityusic Islands displays OSL signals that are dominated by the fast component as shown by the rapid decay during optical stimulation. Also, the shape of the natural OSL signals is similar to the shape of the regenerated signals. The suitability of the samples for equivalent dose determination using the SAR protocol was tested in terms of recycling, infrared (IR) depletion and recuperation tests for each aliquot investigated. Recycling and IR depletion thresholds were set between 0.9 and 1.1. Less than 5% of the investigated aliquots had to be rejected based on these criteria. Recuperation values within 0.2% of the natural signal were exhibited by all the investigated aliquots. The equivalent doses (De) were determined by projecting the sensitivity corrected natural OSL signal onto the dose response curve constructed in each case. OSL signals of these samples display a growth with dose that is best described by the sum of two saturating exponential functions.

Fig. 3 presents a typical OSL decay curve and a dose response curve, depicting the good OSL properties of the investigated quartz.

The ages obtained illustrate that the deposits took place from marine isotopic stage MIS 22 to MIS 6 in the western coast of Eivissa, from the MIS 5 to MIS 3 in Cala en Baster (north east Formentera), MIS 16 to MIS 2 in south Eivissa-Es Freus-Cala Savina (Formentera), MIS 6 to MIS 4/3 in the northern coast of Eivissa, Cala Xuclar-Portitxol, south western coast of Formentera (Es Copinar-Es Ram) from the MIS 5e to MIS 2 (Table 2).

It should be noted that while very high ages (at least from a conventional optically stimulated dating methodological point of view) were obtained and further discussed, this is due to the very low radioactive content of the samples and corresponding dose rate, not the equivalent dose. The equivalent doses obtained for all investigated samples are lower than 250 Gy. **Anechitei-Deacu et al. (2018)** presented extended dose recovery tests on quartz samples from Cala Bassa, by both delivering the artificial doses following bleaching and on top of the natural accrued dose. Their investigations confirmed that equivalent doses of such magnitude (lower than 250 Gy) should be considered reliable, especially when using coarse (>63 μm) quartz. As far as the accuracy of the annual doses is concerned efforts were made to determine the dose rate as accurately as possible. When recording (Fig. 4) the gamma spectra counting was carried out for a very long duration of over 200 ks. In the case of these particular samples checking for radioactive disequilibrium was difficult though, due to the very low radioactivity of the material. However, we consider reasonable to assume that due to the nature of the aeolianite material and its formation, radioactive equilibrium is a fair assumption. The presence of rhizoconcretions (pedodiagenetic mineral accumulations around living ordeal plant roots; **Klappa, 1980**) in the investigated profile (see Cala Bassa) is an indicator for quick cementation. Young ages were reported in literature for aeolianites at different sites, which indicate a rapid carbonate cementation after deposition.

Furthermore, for sample M#26# an intercomparing between gamma spectrometric results and beta counting measurements (**Cunningham et al., 2018**) was performed, the latter analysis being performed at DTU NUTECH. In the case of this particular sample, considering gamma spectrometry measurement results in a beta plus gamma dose rate of 0.258 Gy/ka while for beta counting the obtained value was 0.251 Gy/ka. Thus, the excellent agreement gives us confidence in the obtained results.

4.3. Stratigraphy

Through an analysis of the prominent erosive surfaces and palaeosoils presence, a total of nineteen distinct unconformity-bounded units become evident. These unconformities are discernible across the areas under study, effectively demarcating the aeolian deposits, alluvial/colluvial deposits, marine deposits, and the pedogenetic levels. Aeolian deposits represent the thickest and the most continuous layers in all the studied areas, showing a lateral shift of sedimentary facies due to the orientation of the coast at each study site, as well as the basement palaeotopography.

The lower unit U1 observed at Cap Negret is composed of aeolian facies with interbedded silty palaeosoil layers. This palaeosoil contains levels with subangular and heterometric clasts originating from the basement. The aeolian levels, represented by sand sheets and small parabolic dunes, show lateral changes, being thicker seawards and thinner inland. The foresets show an average NNE dip direction, indicating that the dune migrated inland by the dominant SSW wind direction. The bed dipping angle of cross-stratified increases from 5° to 15° inland. This aeolian deposit overlies a silty palaeosoil.

Unit U2 outcrops in Cap Negret, Punta de Sa Pedrera (Eivissa) and Punta Rasa (Formentera). This unit is composed of aeolian facies and silty palaeosoils. At the top, unit U2 is bounded by an unconformity interpreted as colluvial. Gradual impoverishment in clast size towards upper layers indicates decreasing energy, which is reflected in the continuous upper palaeosoil spreading laterally throughout the unit. The aeolian level is represented by thicker parabolic dunes that evolved to climbing dunes with active migration inland towards ENE direction. Cross-stratified layers have a higher angle upwards of 30° dipping SE; locally in Cap Negret, the angle gradually decreases to horizontal stratification. The direction of migration is oblique to the coast and evolves to climbing dune in the cliff-front formed by the basement. The previous aeolian level in Cap Negret reaches 4 m thick in the area of Sa Punta de Sa Pedrera and migrates inland perpendicular to the coast due to a relief with much less slope than in Cap Negret. The predominant average wind direction was WSW.

Unit U3 is exposed at Cap Negret, Punta de Sa Pedrera, Cala Compte, S'Estanyol and S'Espalmador. This unit consists of two aeolian levels, facies, and colluvial facies. Colluvial facies levels at the base are overlaid by aeolian facies levels resting on an erosive contact. Some thin layers of travertines can be observed at the very top of the unit covering the aeolian sediments. Dune foreset bedding shows an average SE dip direction (25-30°) with a constant thickness in all areas. This indicates a relative change in the prevailing wind direction towards a south component. Additionally, differences in the migration of the dunes are observed according to the study area. Sedimentation is observed in Cala Compte during a predominant wind from the SE due to the orientation and topography of the coast. This sedimentation does not occur on the northernmost side of Cap Negret, Punta de Sa Pedrera, or in Espalmador but occurs during the period with the prevailing wind from the NW.

Table 2
Summary of the luminescence and dosimetry data used for OSL age calculation.

	Sample Code	Depth (cm)	Grain size (μm)	Water content (%)	ED (GY)	U-Ra (Bq/ Kg)	Th (Bq/ kg)	K (Bq/ kg)	Total dose rate (Gy/Ka)	Age (ka)	Total Random error (%)	Total systematic error (%)	MIS
Cala Compte profile	M#15#	1020	63-250	3.0	242 ± 11 n=16	15.3 ± 0.2	2.6 ± 0.3	31.1 ±2.7	0.52 ± 0.01	464 ± 35	4.9	5.8	12
	M#16#	1040	63-250	3.0	240 ± 12 n=14	16.0 ± 0.4	3.3 ± 0.2	34.6 ±3.7	0.57 ± 0.01	422 ± 36	5.6	6.6	12
	M#17#	440	63-250	3.0	215 ± 7 n=12	17.1 ± 0.5	3.0 ± 0.3	38.1 ±3.6	0.64 ± 0.01	337 ± 26	4.0	6.7	10
	M#20#	55	63-250	3.0	78 ± 3 n=9	15.3 ± 0.2	2.3 ± 0.1	12.7 ±3.4	0.59 ± 0.01	131 ± 11	4.3	7.1	6
Cap Negret profile	M#26#	1950	63-250	0.72	224 ± 16 n=7	8.0 ± 0.5	1.5 ± 0.5	8.0 ± 2.1	0.24 ± 0.01	947 ± 100	9.1	5.3	21/ 26
	M#36#	820	63-250	3.0	189 ± 11 n=11	4.8 ± 0.1	1.5 ± 0.2	10.5 ± 3.3	0.25 ± 0.01	747 ± 33	7.1	6.6	18
	M#33#	410	63-250	3.0	213 ± 14 n=11	3.8 ± 0.6	2.0 ± 0.5	17.6 ± 3.2	0.31 ± 0.02	695 ± 77	8.3	7.4	16
	M#2#	260	63-250	3.0	183 ± 11 n=11	9.6 ± 0.7	2.9 ± 0.8	22.0 ± 3.3	0.47 ± 0.02	390 ± 39	7.3	7.0	10
	M#3#	30	63-250	3.0	185 ± 12 n=12	11.6 ± 1.1	4.3 ± 0.1	30.4 ± 4.2	0.61 ± 0.02	292 ± 29	4.8	6.8	8
Punta de sa Pedrera profile	M#5#	850	63-250	3.0	230 ± 17 n=8	13.5 ± 0.5	1.7 ± 0.2	14.6 ±3.6	0.43 ± 0.01	530 ± 52	8.0	5.8	15b /16
	M#4#	420	63-250	3.0	136 ± 6 n=11	10.6 ± 0.2	2.4 ± 0.2	24.8 ±2.7	0.47 ± 0.01	293 ± 23	4.8	6.3	9b
	M#49#	150	63-250	3.0	175 ± 9 n=12	21.4 ± 0.9	3.2 ± 0.3	29.8 ±2.9	0.75 ± 0.02	235 ± 20	5.7	6.3	8
Cala Bassa profile	M#9#	390	63-250	2.0	146 ± 5 n=10	16.5 ± 0.2	2.7 ± 0.5	24.2 ±3.1	0.59 ± 0.01	250 ± 16	4.0	5.7	8/7
	M#6#	355	63-250	4.0	155 ± 9 n=9	16.0 ± 0.6	2.0 ± 0.5	54.9 ±3.0	0.66 ± 0.01	236 ± 16	6.2	5.7	7d
	M#11#	110	63-250	4.0	103 ± 5 n=11	16.2 ± 0.7	2.0 ± 0.6	19.3 ±3.5	0.59 ± 0.02	171 ± 5	5.7	6.2	6
ES Ram profile	M#ES2#	1040	63-90	14.9	220 ± 6 n=11	16.0 ± 0.4	3.3 ± 0.2	34.6 ±3.7	0.51 ± 0.01	120 ±14	3.61	5.41	5
	M#ES7#	440	63-250	15.9	207 ± 5 n=10	17.1 ± 0.5	3.0 ± 0.3	38.1 ±3.6	0.57 ± 0.01	110 ±8	3.29	5.67	5/4
Cala Xuclar profile	M#D1#	350	63-250	1.4	64 ± 6 n=14	11.6 ± 0.1	1.39 ± 0.16	14.4 ±1.2	0.45 ± 0.005	143 ±8	9.44	6.24	6
	M#D2#	160	63-250	0.6	50 ± 1 n=8	12.3 ± 0.2	1.55 ± 0.21	18.0 ±1.4	0.51 ± 0.01	100 ±6	2.36	6.46	5
	M#D3#	105	63-250	3.5	50 ± 3 n=7	12.2 ± 0.1	2.9 ± 0.1	40.6 ±1.3	0.60 ± 0.004	77 ±5	6.05	6.24	4/3
	M#D4#	10	63-250	3.6	57 ± 3 n=10	11.0 ± 0.5	3.8 ± 0.22	67.0 ±2.1	0.75 ± 0.01	73 ±5	5.44	6.63	4/3
S'Estanyol profile	M#60#	310	63-250	9.6	216 ± 21 n=6	11.8 ± 0.5	3.4 ± 0.1	34.8 ±3.7	0.52 ± 0.01	414 ±48	10	6.02	12
	M#63#	170	63-250	10.3	185 ± 16 n=6	7.7 ± 0.1	3.5 ± 0.2	36.8 ±3.6	0.48 ± 0.01	387 ±43	8.93	6.66	10
Es Codolar profile	M#22#	840	63-250	0.7	154 ± 4 n=9	9.8 ± 0.3	4.1 ± 0.2	37.9 ±2.5	0.49 ± 0.01	317 ±20	3.27	5.48	10
	M#24#	730	63-250	18	100 ± 2 n=10	10.1 ± 0.1	3.4 ± 0.1	45.8 ±3.6	0.44 ± 0.01	227 ±15	2.97	5.66	8
	M#26#	220	63-250	14.3	59 ± 2 n=10	9.8 ± 0.2	3.1 ± 0.3	33.7 ±3.1	0.48 ± 0.01	124 ±9	3.93	6.48	6
Ses Salines profile	#SS6#	230	63-250	3	108,3 ± 2 n=10	33,1 ± 0,8	2,00 ± 0,2	63,6± 5,6	0,96 ±0,021	113 ±8	9,4±3,06	41,75±6,46	5
	#SS2#	270	63-250	3	80,1 ± 4 n=10	24,20 ± 0,8	1,00 ± 0,2	39,0 ± 7,0	0,77 ±0,024	104 ±9	30,5±5,52	42,06±6,49	5d
	#SS1#	290	63-250	3	82,5 ± 3 n=11	24,4 ± 0,6	1,50 ± 0,1	9,0 ± 2,0	0,51 ±0,01	163 ±14	16,4±4,0	61,5±7,85	6
	#SS0#	105	63-250	3	79 ± 5 n=10	22,30 ± 1,9	1,8 ± 0,7	15,0 ± 7,0	0,705 ±0,037	112 ±12	67,1±8,19	43,7±6,61	~
Espalmador profile	#MEO#	190	63-250	3	84,9 ± 6 n=8	29,0 ± 0,2	2,20 ±0,40	7±1	0,79 ±0,01	106 ±10	50,9±7,14	61,5±7,85	5d
	#ME1#	1250	63-250	3	169 ± 9 n=10	7.60 ±0.20	1.50 ±0.10	14.0 ±2.0	0,26 ±0,01	665 ±54	35,7±5,9	61,5±7,85	16

(*continued on next page*)

Table 2 (*continued*)

	Sample Code	Depth (cm)	Grain size (μm)	Water content (%)	ED (GY)	U-Ra (Bq/Kg)	Th (Bq/kg)	K (Bq/kg)	Total dose rate (Gy/Ka)	Age (ka)	Total Random error (%)	Total systematic error (%)	MIS
	#ME2#	565	63-250	3	220 ± 12 n=10	22,0 ±0.60	4,00 ±0.60	59,0 ±5,0	0,797 ±0,02	276 ±24	36,3±6,03	42,06±6,49	8/7
	#ME3#	80	63-250	3	226,6 ± 11 n=10	17,90 ±0.40	32,00 ±1,00	38,0 ±6,0	1,22 ±0,03	183 ±15	27,9±5,29	39,8±6,32	6
	#ME4#	50	63-250	3	109,4 ± 3 n=9	22,40 ±0.60	5,00 ±0.90	87,0 ±6,0	1,01 ±0,025	108 ±8	12,1±3,48	42,7±6,54	5d
Cala en Baster profile	#CB1#	1100	63-250	3	72 ± 5 n=10	32.3 ± 0,3	1,4 ± 1,0	22,4 ± 5,3	0,957 ± 0,023	91 ± 9	46,5 ± 6,82	43,03 ± 6,56	5c
	#CB3#	420	63-250	3	59 ± 3 n=9	28,0 ± 1,4	2,4 ± 0,9	30,0 ± 4,6	0,830 ± 0,030	72 ± 7	43,2 ± 6,57	41,5 ± 6,44	4
	#CB4#	35	63-250	3	64 ± 3 n=10	27,6 ± 0,5	2,6 ± 1,0	36,2 ± 5,2	0,924 ± 0,024	70 ± 6	27,1 ± 5,20	43,2 ± 6,57	4/3
	#CB5#	20	63-250	3	66 ± 2 n=10	22,2 ± 0,3	4,8 ± 0,9	71,4 ± 5,1	0,983 ± 0,022	67 ± 5	10,2 ± 3,2	43,8 ± 6,62	4/3
	#CBP#	1000	63-250	3	139 ± 2 n=10	36,5 ± 0,5	25,7 ± 4,4	358,1 ± 17,3	1,672 ± 0,053	83 ± 7	12,7 ± 3,57	49,8 ± 7,06	5b
Illa d'es Penjats profile	#IP2#	350	63-250	3	71,3 ± 1,7 n=10	33,8 ± 3,1	28,9 ± 1,2	31 ± 8	0,82 ±0,029	87 ±7	118,8 ±4,33	41,7±6,5	5/4
Illa d'es Porcs profile	#IPC3#	70	63-250	3	47,4 ± 0,6 n=10	27,1 ± 0,2	33,2 ± 0,8	476 ± 14	2,67 ±0,046	18 ±1	4,6±2,1	46,6±6,8	1/H
	#IPC1#	300	63-250	3	81,6 ± 3,9 n=10	23,7 ± 2,1	25,6 ± 0,8	32 ± 7	0,79 ±0,026	103 ±9	34,1±5,8	41,6±6,45	5
	#IPC2#	20	63-250	3	71,3 ± 1,8 n=9	27,1 ± 0,2	24,4 ± 0,8	26 ± 6	0,83 ±0,021	86 ±7	13,2±3,6	45,9±6,8	5/4
Illa d'es Caragol profile	#IC1#	350	63-250	3	75,3 ± 1,9 n=9	35,10 ± 1,1	35,1 ± 1,10	16 ± 6	0,89 ±0,025	84 ±6	14,4±3,8	41,5±6,44	5/4
	#IC2#	180	63-250	3	75,6 ± 2,7 n=9	18,7 ± 2,5	27,3 ± 0,9	35 ± 5	0,83 ±0,019	91 ±7	18,3±4,3	42,1±6,5	5
Cala Sabina profile	#CS1#	220	63-250	3	92,1 ± 10,1 n=10	31,9 ± 1,2	31,9 ± 1,2	48 ± 8	0,98 ±0,029	94 ±12	129,2 ±11,4	41,9±6,47	5
Es Portitxol profile	#MP1#	105	63-250	3.08	96,0 ± 5 n=12	10,8 ± 0,6	10,8 ± 0,6	16,0 ± 2,0	0,541 ±0,014	178 ±15	33,7 ± 5,81	37,9 ± 6,16	6
Punta Rasa profile	#MF1#	1500	63-250	4.17	232 ± 7 n=18	11.9 ±0.70	1.50 ±0.10	9.0 ±2.0	0,297 ±0,012	781 ±59	25,8 ± 5,08	31,1 ± 5,58	22/18

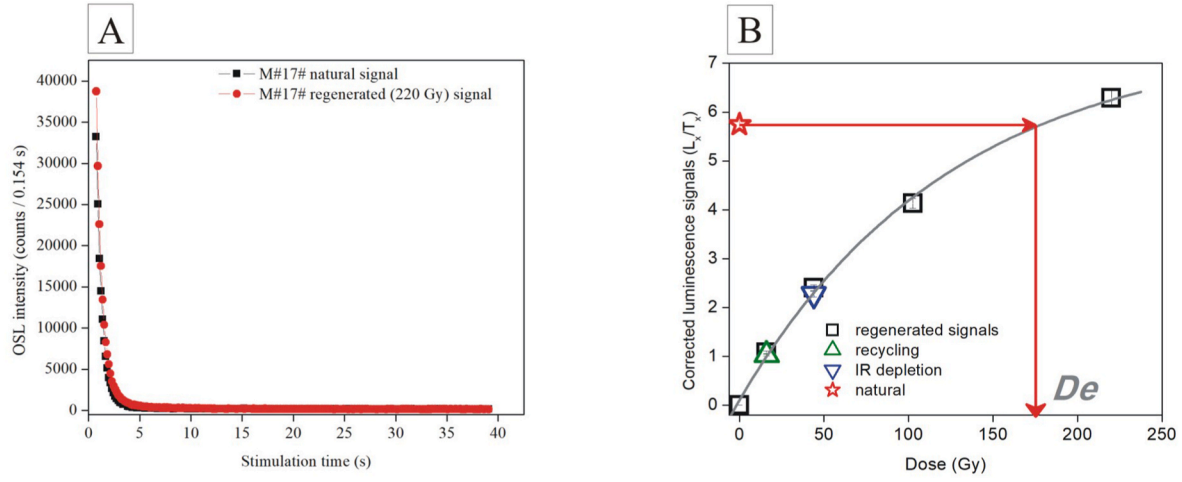

Fig. 4. A) Typical decay curve of natural CW-OSL signal (black squares) in comparison to a regenerated (laboratory dose) signal (blue circles). B) Representative sensitivity-corrected growth curve constructed for sample M#CB3# using one aliquot of coarse (63–250 μm) quartz grains. The regenerated doses are shown as black open square The sensitivity corrected natural signal is depicted as a star and the equivalent dose is indicated by arrows. Recycling and IR depletion points are represented as up and down triangles.

Also, this sedimentation occurs in s'Estanyol area, where the dunes are thinner than in all the other areas. This unit is interpreted as a parabolic dune field migrating inland. The aeolian levels change in thickness and are separated by several palaeosoil lenses.

Unit U4 can be divided into two sub-units (U4a and U4b). U4a was observed in Cala Compte outcrops and is composed of aeolian facies and clayey palaeosoil. The parallel and perpendicular view of the aeolian level to the coast shows an internal structure with a dip angle of SE. This suggests that this dune is parabolic and migrates obliquely to the coast –SE-with a predominant wind direction of the NW.

On the other hand, sub-unit U4b is observed in Cala Compte and S'Estanyol and is composed of the aeolian facies and different types of palaeosoils. In the upper part of the unit, calcretes levels with pisoliths are observed. This unit represents a parabolic dune field migrating inland –NW- towards the Cala Compte area. The cross-stratified layers have angles higher than 30° dipping NW, which gradually decrease to horizontal stratification 5° NW. This dune indicates a predominant wind change of NW to SE, due to the orientation of the coast of Cala Compte towards the W-SW. This unit is only found in Cala Compte and S'Estanyol, as the other study areas are protected by the island of Sa Conillera.

Unit U5 is observed in the Cala Compte, Cap Negret, S'Estanyol and Es Codolar outcrops, and it consists of aeolian facies and different palaeosoils. The aeolian levels increase in thickness towards the cliff front, showing high angle cross-stratification up to 35° with foreset indicating a prevailing wind NW- WNW in Cala Compte, Cap Negret and Es Codolar, but a different prevailing wind direction of the ESE is observed in the S'Estanyol area. Levels of palaeosoils with concave-up forms interbedded in the aeolian levels, possibly formed in the interdunar depressions (dune corridors), are observed. The aeolian facies in this unit present local differences, especially in the aeolian thickness, being thicker in Cala Compte and smaller in Cap Negret. This is due to the prevailing wind at the time of the formation of the dunes, which were of the NW. The most obvious reason is the orientation of the coast and the presence of the island of Sa Conillera, a small island that acts as a barrier over the area of Cala Bassa and Punta de Sa Pedrera from the winds of the west. It should also be noted that these areas are oriented to the north and north-east, while the S'Estanyol area is oriented to the SE.

Unit U6 is present in the Cap Negret and Punta de Sa Pedrera outcrops and consists of sandy palaeosoil and an aeolian facies. This level is represented by small parabolic dunes. Dune foreset bedding shows an average NW. Additionally, the sandy palaeosoil increases in thickness almost 1.5–2 m in Cap Negret and presents abundant carbonate nodules. The prevailing wind at this moment remained the same as in the previous unit –SE-SSE-, with some slight changes depending on the orientation and topographic features of the area, but not very noticeable. Although, there is a remobilized part of the sand from the previous features.

Unit U7 is present at outcrops in Punta de sa Pedrera, Cala Bassa, Es Codolar and Espalmador. It is composed of aeolian facies and a sandy palaeosoil. West of Punta de sa Pedrera, a palaeosoil with mudcracks is observed, resting on top of a level of calcretes. Up on this level is a unit of aeolian facies represented by small superimposed parabolic dunes migrating inland toward the ESE, indicating a prevailing wind direction from WNW. Between the overlying dunes, there are lens-like shaped pedogenetic levels interpreted as small interdune ponds.

Unit U8 was only observed in the Cala Bassa outcrop. This unit is composed of aeolian facies and two palaeosoils. The aeolian facies is interpreted as a parabolic dune migrating inland in Cala Bassa and transforming to small climbing dunes inland with a migration direction of SSW. The cross-stratified layers show angles 5-15° which gradually decrease to horizontal stratification. The thickness of this level decreases as it migrated inland, controlled by the presence of smooth coastal valleys or hill ridges. The main reason why one can only find these dunes with inland migration at the coast of Cala Bassa perpendicular to the coast is due to its orientation facing a predominant wind from the N and NE.

Unit U9 was observed in Cala Bassa, Cala Compte, Ses Salines, Espalmador, Es Codolar, Cala Xuclar, Es Portitxol and Cala en Baster outcrops. This unit is separated from unit U8 by an erosive unconformity. The facies architecture and succession patterns of the deposits show three clear aeolian sub-units separated by palaeosoils (U9a, U9b, and U9c). The sub-unit U9a is composed of the aeolian facies and a palaeosoil, while sub-unit U9b is composed from the aeolian facies and the palaeosoil. Sub-unit U9c is composed of aeolian facies and a sandy palaeosoil. The aeolian facies represent field dunes composed of small, superimposed dunes. The thickness of these deposits decreases inland, and the paleocurrent analysis provides an aeolian transport to SSE. Cross-stratified layers have an angle upwards 25° dipping South (20-25/085), indicating a predominant wind direction of the NNW - NNE. Also, differences in the grain size of some levels of the dunes present in the two areas indicate moments of greater intensity of the predominant wind of the period.

Unit U10 is composed of marine levels present in Es Copinar-Es Ram, the eastern part of S'Espalmador, and Cala Savina study areas, about half to 1 m above the current sea level, with a large amount of marine macrofauna. It is worth nothing the presence of thermophile fauna such as *Thetystrombus latus* (Gmelin, 1791) (ex. *Strombus bubonius*) belonging to the interglacial isotopic stage of MIS 5e. Also, due to the warm and humid conditions, interdune lagoons were formed, especially in Ses Salines.

The next unit U11, corresponds an aeolian phase in Ses Salines, Espalmador islet, also in Cala Xuclar and Illa des Porcs. Also, palaeosoils were formed in the upper part of the small parabolic dunes in S'Espalmador, Es Freus, Cala Savina, Cala Xuclar, Es Codolar, Ses Salines and Es Copinar-Es Ram. Above this level, there is a beach level (shallow-marine unit- U12) that is formed by sandy matrix with a large amount of marine fauna with a predominance of *Glycymeris violacescens*.

The uppermost part of the second beach level is partially eroded in all the study areas. This change from a sandy matrix to a silty red matrix interpreted as an erosive surface (U13) that developed during the sea level regression. On top of this level, aeolian dune deposits are observed. The structure and arrangement of the layers from these units indicates wind flow prevailed from the NE-NNE in Es Copinar-Es Ram. However, these dunes are partially or totally eroded throughout the study area by a sandy colluvial unit U14 (sandy channels) with the presence of angular clasts, especially in the form of lenticular channels. This colluvial surely formed during unstable weather or wetter episodes.

The next unit U15 consists of aeolian dune deposits, present in Cala en Baster, Es Copinar-Es Ram, Cala Xuclar, Illa des Penjats, Illa des Porcs and Illa d'es Caragol. It is characterized by the presence of a thick dune package bounded at the base by an unconformity that overlaps the previous units during their inland migration. In Es Copinar-Es Ram and Cala Xuclar, the dunes evolved to climbing dunes, while in other areas, they evolved to parabolic dunes. The structure and arrangement of the layers from these units indicate that wind flow prevailed from the SW-SSW in the Es Freus islets and Formentera, and a prevailing wind direction of the N-NW in the northern coast of Eivissa and from the N-NE in Cala en Baster in Formentera. These winds would have caused dune migration over the colluvial unit U14.

The damp interdunar deposits in Es Copinar-Es Ram over the unit U15 are interpreted as indicating minor sediment availability compared to the previous unit, as the unit thickness continuity along the Pleistocene successions suggests. The unit U16 is a colluvial/reworked unit present in Cala en Baster, Cala Savina, Ses Salines, Cala Xuclar and Es Copinar-Es Ram. It is bounded at the base by an unconformity, and at some points, the sand-sheet deposits have been eroded by fluvial activity and channelized flows.

The unit U17, present in Cala en Baster and Es Copinar-Es Ram, is composed by silty-sandy matrix with abundant migrating channels, which are very tight and partially or totally eroded the sandsheets. The clasts in this unit originate mainly from the basement and part of the lower levels. The overlapping of the clasts presents in the channels,

indicates that the migrate or are formed from the land to sea and often even invade the marine platform.

The penultimate unit U18 is formed by a colluvial present in Es Copinar-Es Ram, Cala Xuclar and S'Espalmador. The deposits show a red silty matrix with an erosive contact and angular clasts ranging in size from centimetres to larger sizes. There are also two levels of calcretes, each 0.5–1 m thick in the lower and upper parts of the level. The last unit, U19, is composed by a thick dune field present in Es Copinar-Es Ram. The internal structure indicates that this level migrated inland with the prevailing wind of the W-SW.

5. Discussion

Carbonate aeolian deposits, colluvial deposits, marine deposits, and palaeosoils are all typical features of the Pleistocene sediments along the coast of the Pityusic Islands. These sedimentary successions are the result of eustatic oscillations related to glacial and interglacial periods, as well as relatively rapid warming and cooling episodes (**Lowe and Walker, 2015**). During interglacial periods, pre-existing deposits were eroded and recycled, leading to the development of beach levels on narrow shore platforms cut by waves. During cooling periods, colluvial and alluvial deposits formed on the coasts, along with aeolian deposits resulting from the onset of dune migration inland as sea level dropped and the continental shelf became exposed (**Pavelic et al., 2011**; **Andreucci et al., 2014**). With the onset of glacial climate conditions, extensive dune fields moved to the coast on the shelf (**del Valle, 2016**; **Pomar, 2016**). Geomorphological processes such as beach formation, alluvial fans, and dune fields that operate on the coast are conditioned by the sea level response to the availability of sediment and the existence of enough space for the development of the processes that generate these fluctuations (Miall, 1996, 2010; **Muto and Steel, 2000**).

Sedimentological analyses performed on several sandstone levels have shown that the main source of these sediments is marine sands, and that the aeolianites are made up by of well-sorted bioclastic sands, indicating that the source area was the coastal zone. The mineralogical composition of the sediments is predominated calcite (>80 %). The sediment composition shows a predominant presence of carbonate skeletal fragments, as mollusc shell fragments, echinoderms, red algae, foraminifera, briozoans, as well as some lithoclasts.

During warmer periods, Northern wind influxes were reduced, generating lower pressures formation on the western Mediterranean and boosting warm African air masses from the South (**Kaspar et al., 2007**; **Moreno et al., 2002**; **Bardají et al., 2009**). These African air inputs often generate dust rains, which may constitute most of the Balearic soils composition (**Fornós and Ahr, 1997**; **Moreno et al., 2002**; **Fornós et al., 2004**; **Fiol et al., 2005**; **Muhs et al., 2010**). Temperature increase and sea level rise favours vegetation growth and soil formation.

The morphology of the coastal relief, comprising of cliffs shaped by folded Lower Jurassic rocks and Miocene conglomerates, along with changes in wind direction, controlled the overall architecture of the sedimentary bodies. The cliffs morphology and the irregular position of the small catchments that reach the shoreline exert secondary local control on sedimentation processes, and consequently, facies development and location. These changes in wind patterns interact with the relief and coastline orientations, resulting in local changes in sedimentary body thickness and facies. These factors create a complex architecture with significant lateral variability. The observed sedimentary sand bodies architecture allows to differentiate four majors sedimentary aeolian environments: climbing and cliff-front dunes, parabolic dunes, transverse dunes, and sand sheets. Therefore, the dune formation is mainly controlled by the sea level, which provides accommodation space and sediment availability. Still, the type of dunes is influenced by the relief, including the orientation of the coast and terrain ruggedness, interacting with the prevailing wind of the moment.

The sedimentological investigations and the OSL chronology presented in this study, along with the OSL dating provided by **Bardají et al., 2017**), allow for constraining the main aeolian episodes and reconstructing the landscape evolution of western Eivissa between 800 and 900 ka and 14 ka (MIS 22 to MIS 2). Nineteen differentiated units indicate almost fourteen aeolian sedimentation periods, pointing out to arid environmental conditions associated to sea level dropping. These arid conditions are also evidenced by the punctual presence of calcretes and pisolith horizons (**Flügel, 2014**). These aeolian sediments are separated by palaeosoils representative of warmer and relatively wetter conditions. Silty-clayey palaeosoils, which in some cases have high bioturbation and reddish coloration due to rubefaction, indicate an increase in precipitations (**Wagner et al., 2014**). Conversely, the presence of travertines with laminar structures could indicate the existence of water flowing conditions (**Claes et al., 2015**; **Toker et al., 2015**).

In this study, we leverage the marine isotopic record as a robust analytical tool, owing to its global applicability and widespread recognition within the scientific community. The inherent global character of the marine isotopic record renders it an invaluable resource for establishing a unified chronological framework, facilitating the correlation of events across disparate geographical locations. Our focus on correlating Pleistocene deposits in the present case study with the marine isotopic record serves as a method to authenticate regional paleoclimatic records. The alignment of local variations with the globally consistent marine isotopic signal enhances confidence in the precision and reliability of these paleoclimatic records. Additionally, we explore the influence of Milankovitch cycles on the marine isotopic record, particularly the 100,000-year glacial cycles driven by eccentricity (Rodrigues et al., 2017; Bajo et al., 2020; Gibbard and Hughes, 2021). Our investigation reveals a compelling connection between these Milankovitch cycles and the arid phases recorded in the dune systems of the Pityusic Is. (MIS 22-14). Specifically, the cold stages of glacial cycles emerge as key drivers of the global hydrological cycle, elucidated by the geomorphological and paleoenvironmental evidence presented by the Pleistocene aeolian deposits of the Pityusic Is. Furthermore, the incorporation of Optically Stimulated Luminescence (OSL) dating enhances the temporal precision of these arid periods, contributing to a more nuanced understanding of the climatic dynamics during the Pleistocene era.

Regarding the evolution of the Pityusic islands, it is known that the first aeolian level was dated to 947 ± 100 ka (MIS 22) (Fig. 5 A). This level corresponds to the unit U1 observed in Cap Negret and Punta de sa Pedrera (Eivissa) and Punta Rasa (Western coast of Formentera) outcrops. These form the coastal cliffs or the base of the Pleistocene deposits. Based on the OSL data and the error range, this level may correspond to the marine isotopic stages MIS 22 or MIS 18. During both marine stages the sea level dropped (**Silva et al., 2009**).

The second aeolian level (unit U2) based on the OSL presents an age of 747 ± 33 ka (M#26# Cap Negret) and 781 ± 59 ka (M#F1# Punta Rasa). The unit U2 is referred to the isotopic stage MIS 18 (Fig. 5B). The absence of rizhoconcretions is interpreted as a lack of vegetation and therefore dunes were probably formed during a very arid period.

In the different outcrops this dune level is superimposed on the previous aeolian level as well as on the basement. The rising sea level interrupted the formation of dunes and favoured the formation of soils. Some sections show palaeosoils that could correspond to this moment of biostasis. On top of this pedogenetic complex small parabolic dunes can be observed sometime overlapping the mentioned soil, indicating an aeolian pulse.

Above the second dune phase lies a colluvial level with characteristic architecture of floodplain-hillslope deposits and typical forms of channelized flows. It interfingers two aeolian levels dated to 747 ± 33 ka (M#36#, Cap Negret) and 695 ± 77 ka (M#33#, Cap Negret), corresponding to MIS 18 and MIS 16, respectively. Thus, it is reasonable to assume that these sediments were deposited during MIS 17. This isotopic stage is characterized by a lowstand phase. This scenario indicates environmental conditions changing towards a warmer and wetter climate that could correspond to an interglacial stage.

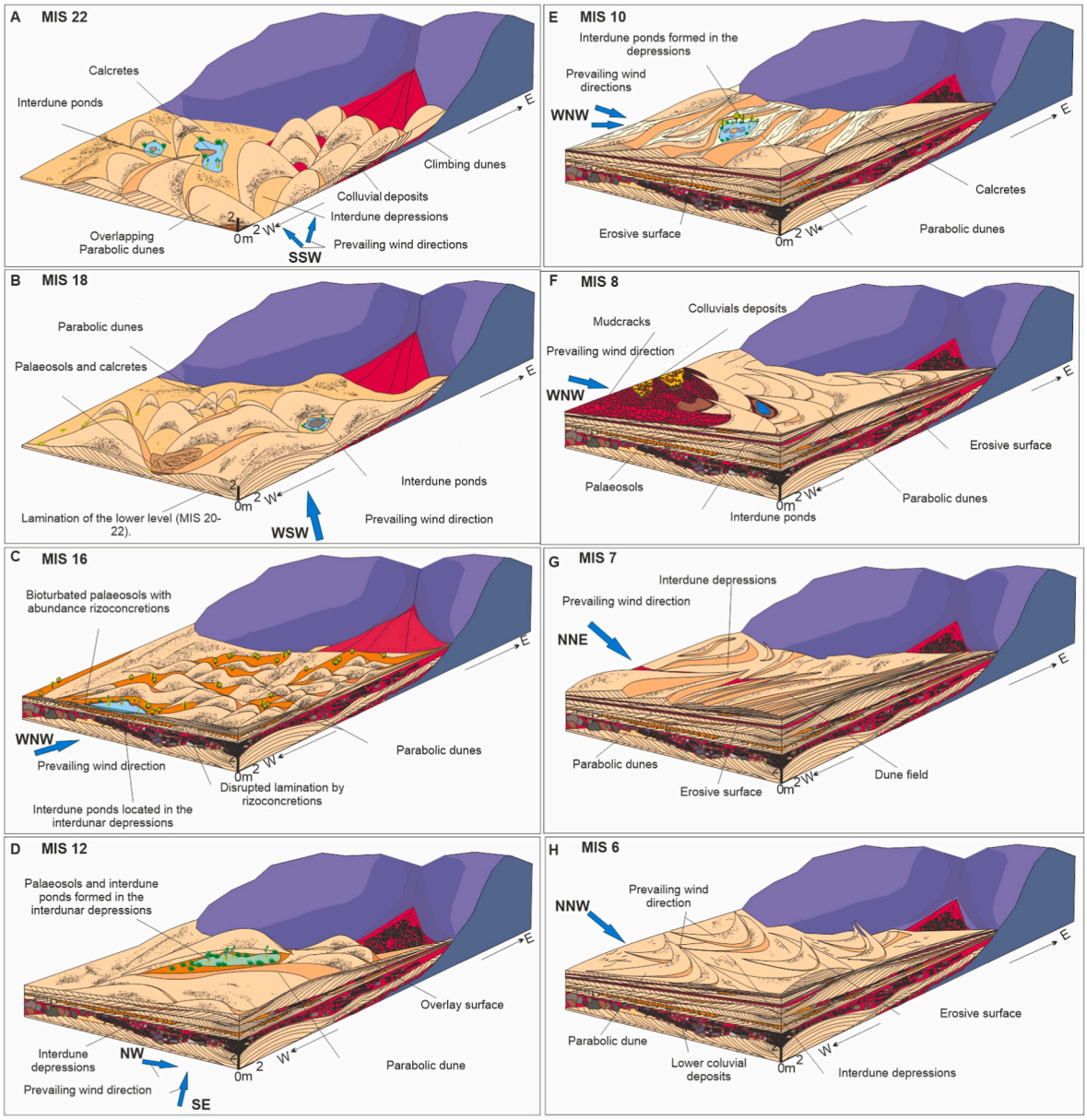

Fig. 5. Depositional environment evolution model showing the succession of the main sedimentary environments and paleocurrent directions of the western coast of Eivissa from MIS 22 to MIS 6.

The third period of dune fields formation in the western coast of Eivissa, S'Estanyol and Espalmador (Figs. 5C and 6A) is characterized by a thick aeolian level interbedded between the colluvial level described above and a palaeosoil. These aeolian levels representing parabolic dunes and belonging to unit U3 were dated to 695 ± 77 ka (M#33#) (MIS 16), 530 ± 52 ka (M#5# Punta de sa Pedrera), and 651 ± 52 ka (#ME1# Espalmador). This isotopic stage is characterized by a progressive decreasing sea level (Silva et al., 2009). Lamina of the upper part of the dunes are very altered by vegetation, displaying remains of rizhoconcretions that are very calcified, suggesting lesser arid conditions than for the previous dune phases. The colluvial level represented by sheet-flood deposits within unit U3 represents the most distal part of a colluvial fan and registers scarce mass movements near the cliff foot that probably occurred after heavy rainstorms.

Changes in the environmental conditions are represented by the development of silty-clay palaeosoils above the dune level. This is supported by the presence of a travertine level in the Cap Negret area and Cala Compte, which could be related to abundant water contribution and circulation, as well as to the probable increasing temperature (Claes et al., 2015; Toker et al., 2015). These factors likely ascribe these travertines and palaeosoil levels to the warm period of MIS 15 or MIS 13. There is evidence that during the transition from the glacial period MIS 16 to MIS 15, the sea level suffered a sudden rising level (Silva et al., 2009).

The fourth period of aeolian sedimentation observed on the western coast, in S'Estanyol and in Espalmador islet (unit U4) was dated to 464 ± 35 ka (M#15#, Cala Compte), 414 ± 48 ka (S'Estanyol M#60#) and 422 ± 36 ka (M#16# Cala Compte), corresponding to MIS 12 (Figs. 5D and 6C). The aeolian levels observed between lower silty levels reach the largest thickness of the studied aeolian deposits. During MIS 12 a sea level dropped -lowstand phase- (Waelbroeck et al., 2002; Rohling et al., 2009; Silva et al., 2009). According to the sea level curve presented by Waelbroeck et al. (2002), during MIS 12 two regressive peaks occurred: the first peak (MIS 12a) occurred at around 460 ka and the second (MIS 12b) at 430 ka. The OSL dating results suggest that there were two periods in which there was an important aeolian

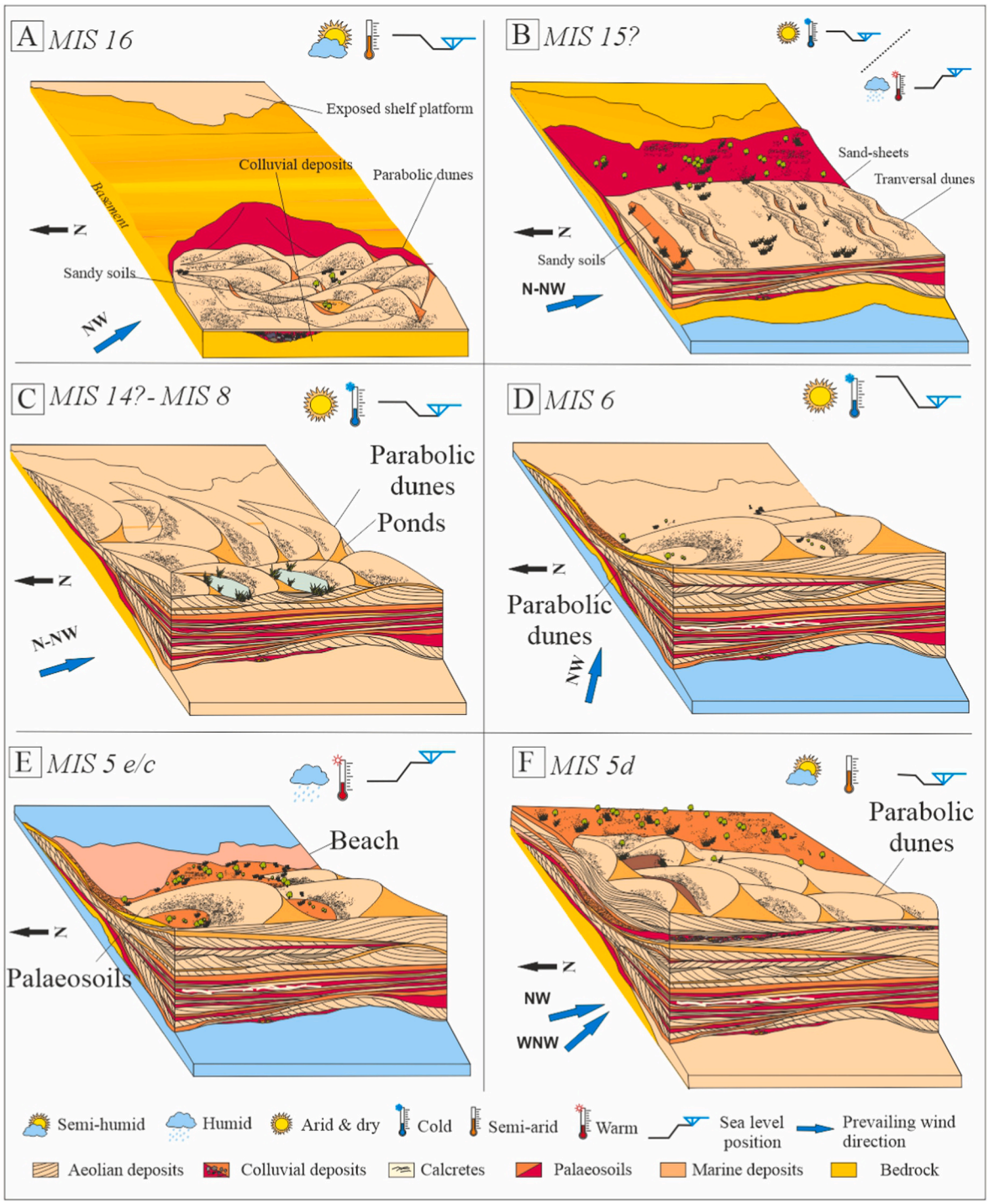

Fig. 6. Depositional environment evolution model showing the succession of the main sedimentary environments and paleocurrent directions of the Es Freus islets from MIS 16 to MIS 5d.

sedimentation with the formation of climbing dunes of 1–5 m thick (unit U4) during the MIS 12. Palaeosoils with a high vegetation concentration are observed in the interdune spaces. These palaeosoils probably represent small ponds formed in wetter periods.

The next period of aeolian activity (unit U5) was dated to 331 ± 27 ka (M#17# Cala Compte), 317 ± 20 ka (Es Codolar #M22#), 387 ± 43 ka (S'Estanyol #M63#) and 390 ± 39 ka (M#2# Cap Negret) and corresponds to MIS 10 (Fig. 5E). This period is characterized by a low marine level (**Silva et al., 2009**). This period of aeolian sedimentations reflected in the complex field of parabolic dunes that suggests a long arid period altered with short stable and humid periods represented by palaeosoils. Other aeolianites dated by OSL and magnetostratigraphic analysis from the near island of Mallorca, corresponds to this isotopic stages MIS 10 (**Nielsen et al., 2004**). During the transition from MIS 10 to the MIS 9 there was a rapid rise of the sea-level reaching up to 1 m above the present (**Zazo, 2006**). During this stable and warm period, soils proliferated. The sixth aeolian sedimentation period observed is represented by a thin aeolian level (unit U6) located above a sandy-silty level dated to 292 ± 29 ka (M#3#, Cap Negret) and 293 ± 23 ka (M#4# Punta de sa Pedrera). It corresponds to the isotopic stage of MIS 9,

probably to the regressive stage of MIS 9b (295 ka). During this interglacial, sea level was probably close to the present level. But in the regressive stage of MIS 9b the sea level dropped (Rohling et al., 2009; Waelbroeck et al., 2002). Other similar aeolian deposits have been described in the eastern part of the Mediterranean (Egypt) by El-Asmar and Wood (2000) and corresponds to the MIS 9. The seventh aeolian period is represented by a thick aeolian level, interbedded between colluvial deposits and palaeosoils (unit U7) dated to of 235 ± 20 ka (M#49#, Punta de sa Pedrera), 250 ± 16 ka (M#9# Cala Bassa), 227 ± 15 ka (M#24# Es Codolar) and 276 ± 24 ka (#ME2# Espalmador). This aeolian sedimentation period corresponds to MIS 8 (Fig. 5F). Studies related to the depositions of phreatic speleothems in coastal caves of Mallorca, during the isotopic stage MIS 8 reflect a sea level drop up to 23 m below the present sea level (Ginés et al., 2001; Dumitru et al., 2020). During that period parabolic superimposed dunes developed under a prevailing west wind. Aeolianites appertaining to this period are also described in the neighbouring island of Mallorca (Nielsen et al., 2004).

The eighth phase of aeolian sedimentation documented in outcrops from Cala Bassa and Cala Compte (unit U8) is represented by an aeolian level located above a silty level with an age of 236 ± 15 ka (M#6# Cala Bassa), corresponding to the isotopic stage of MIS 7, and particularly to the regressive stage of MIS 7d (230 ka) (Fig. 5G). During MIS 7, which represents a warm episode, two regressions peaks occurred (7d and 7b). According to Shackleton and Vincent (1978) and Zazo (1999), the sea level during the MIS 7 was lower than the present sea level. On the contrary, during the highstands of the MIS 7 (7e, 7c and 7a) where the sea level was high a prograding beach system formed in Sardinia (Andreucci et al., 2009). Also, some deposits from Mallorca mark a high sea level during MIS 7a (Tuccimei et al., 2000); other studies from Alicante (Goy et al., 2015) and Tipasa (Authemayou et al., 2016) reinforce this theory from studies of beach sediments (i.e. U. Series-*Cladora corals*) (Table 3).

The ninth aeolian activity (unit U9) observed on the west, south and north coast of Eivissa, Cala en Baster and Espalmador documented here, corresponds to the penultimate glacial stage MIS 6 based on obtained ages of 172 ± 12 ka (M#11# Cala Bassa) 131 ± 11 ka (M#20# Cala Compte), 163 ± 14 ka (M#SS1# Ses Salines), 124 ± 9 ka (M#26# Es Codolar), 143± ka (M#D1# Cala Xuclar), 178 ± 15 ka (M#P1# Es Portitxol) and 183 ± 15 ka (#ME3# Espalmador) (Figs. 5H, 6D and 7A). This period is characterized by a low marine level (Sidall et al., 2003; Rabineau et al., 2006; Silva et al., 2009). During this glacial stage, parabolic dunes were formed. Aeolian deposits formed during the MIS 6 have also been described in other areas of the western Mediterranean, including the Balearic Islands (del Valle et al., 2016; 2020a,b,c; Pomar et al., 2018), Sardinia (Andreucci et al., 2009; Pascucci et al., 2014) but also in the eastern of the Mediterranean, concretely from the Israel coasts (Sivan et al., 1999; Frechen et al., 2004; Mauz et al., 2013).

Unit U10 corresponds to a beach level located in the eastern part of s'Espalmador, Cala Savina and Es Copinar –Es Ram, about 1 m above the current sea level (Figs. 6E and 8A). According to Butzer and Cuerda (1962); Nolan (1895) this beach level has the chronostratigraphic macrofauna senegalenses (*Thetystrombus latus* ex. *Strombus bubonius*), this corresponds to the maximum interglacial MIS 5e. During this period sea level reached +3 m asl, associated to the first Late Pleistocene highstand and represented by the presence of warm fauna considered as a biochronostratigraphic marker (i.e. *Thetystrombus latus*), because this Senegalese fauna immigrated into the Mediterranean during the MIS 5 and disappeared with average sea-surface temperature falling below 20 °C (Sessa et al., 2013; Mauz et al., 2020). Therefore, the assemblage disappeared most probably ~115 ka, but may have been remained until ~80 ka in along the warm north African coast. At some locations around the Mediterranean coasts there is evidence of sea-level highstands, corresponding to the isotopic stage MIS 5e, beach deposits such as in Mallorca (Cuerda, 1989; Vicens, 2015), Italy (Ferranti et al., 2006), Sardinia (Andreucci et al., 2009; Andreucci et al., 2010b; Pascucci et al., 2014), Liguria (Federici and Pappalardo, 2006; Carobene, 2015), Calabria (Dumas et al., 2005, Cerrone et al., 2021), Tuscany (Mauz, 1999; Ferranti et al., 2006), Rome (Mauz et al., 2020); Plugia (Boenzi et al., 1985; Dai Pra and Hearty, 1988; Mastronuzzi et al., 2007), Taranto (Amorosi et al., 2014), Venice (Donnici and Serandrei Barbero, 2004; Tosi et al., 2007b) Sicilia (Antonioli et al., 2006) Algheria (Authemayou et al., 2016), Oran (Meghraoui et al., 1996) Egypt (El-Asmar and Wood, 2000). South Spain (Bardají et al., 2009; Mauz et al., 2012); Morocco (Alouane, 2001; Occhietti et al., 2002; Poujol et al., 2014), Tunisia (Jedoui et al., 2002; Mauz et al., 2012) or Israel (Frechen et al., 2004; Mauz et al., 2012), with the common characteristic of the presence of warm "senegalensis" fauna. Beach levels belonging to MIS 5e have also been described around the world, e.g. South Africa (Jacobs and Roberts, 2009; Cawthra et al., 2018); Bahamas (Hearty and Neumann, 2001; Carew and Mylroie, 2008); Australia (Hearty and O'Leary, 2008) among others or such as the phreatic overgrowths on speleothems from Mallorca (Tuccimei et al., 2006; Dorale et al., 2010; Polyak et al., 2018; Dumitru et al, 2021).

The tenth aeolian phase with an age of 104 ± 9 ka in Ses Salines, and ages of 106 ± 10 ka and 108 ± 8 ka obtained in S'Espalmador, ages from Cala Xuclar 100 ± 6 ka and from Illa des Porcs 103 ± 9 ka, corresponds to the unit U11. These ages indicate its formation during the regressive substage MIS 5d (Fig. 6F). Surely it began to form during the descent of the sea level. Evidence of this substage is present in Mallorca speleothems (Tuccimei et al., 2006; Vesica et al., 2000) and alluvial deposits from Sardinia (Pascucci et al., 2014) or Libia (Macklin et al., 2002).

On the contrary, during interglacial highstands, more precisely during MIS 5c, a beach system developed on the coastal plains, dominated by wide sandy beaches rich in macrofauna (*Glycymeris violacescens; Arca noae; Patella rustica; Conus ventricosus, etc.*) (U12). This Beach level is observed in Cala en Baster (del Valle et al., 2020a,b,c), Es Copinar-Es Ram and also in Cala Savina and probably formed during the highstand MIS 5c, because the stratigraphy, faunal content and mineral composition, together with absolute dates, this level correlates very well in the outcrops mentioned above (Figs. 7B and 8B). Palaeosoils were also formed in the upper part of the small parabolic dunes in the western part of s'Espalmador, Cala Savina, Cala Xuclar, Es Codolar and Ses Salines. Locally, in Es Copinar-Es Ram, this level evolved into a colluvial level due to a erosive period during the sea level regression during MIS 5c to MIS 5b. On the neighbouring island of Mallorca similar palaeosoils have been studied and interpreted as reflecting periods of warmer temperatures and variable conditions of aridity and vegetation cover related to periods of hightands (Wagner et al., 2014; Rose et al., 1999). In this sense, a variable number of highstands has been reported from the Spanish coasts during the MIS 5c (Fornós et al., 2012), in Italy, concretely in Ligura NW (Pappalardo et al., 2013); in Rome (Mauz et al., 2020), in Calabria (Cerrone et al., 2021), in Tuscany Central-Western Italy (Mauz, 1999) in Sardinia (Andreucci et al. (2009, **2010a**, **2010b)**; Tunisia (Nathan and Mauz, 2008); Israel – Carmel Coast- (Sivan and Porat, 2004) and Alexandria -NW Aegypt- (El-Asmar, 1994; El-Asmar and Wood, 2000). Over the beach level calcretes with soft-sediment structures characterized by load casts were observed, together with insect trace fossils, root casts, etc. These developed in several aggrading stages. Dust and/or alluvial-colluvial deposition during arid periods alternated with carbonate leaching and precipitation form the palaeosoils during more humid stages when plants, insects and bacteria played a role in calcretes formation (Huerta et al., 2015). During the MIS 5c palaeosoils were formed in the upper part of the small parabolic dunes. The changes in environmental conditions generated episodes of intense rainfall that together with the change in the base level formed important runoff processes of slopes, favoured by the lack vegetation, eroding the previous soils formed during the warm stage and deposition these sediments as a colluvial on the coastal plains.

During the substadial MIS 5b aeolian dune are developed in Es Copinar-Es Ram and in the Illa des Porcs, this is confirmed from the OSL

Table 3
Previously published Pleistocene data, from sites within the Mediterranean.

Reference	Region	Country	Site	Original description	Time	Dating
Bardají et al., 2009	Western	Spain	Mallorca	Plesitocene beach rock dep.	MIS 5e	
Dorale et al., 2010	Mediterranean			Phreatic overgrowth on Speleothems(POS)	MIS 5e, 5a	
Fornós et al., 2002				Dunes	MIS 3	
Fornós et al., 2007				Dunes	MIS 1	
Fornós et al., 2009				Dunes	MIS 5c/b, 4, 3	OSL
Nielsen et al., 2004				Dunes and pedogenetic deposits	MIS 10, 8	OSL; Magnetostrastrigraphy
Polyak et al., 2018				POS	MIS 5e, 5a	U-Th
Rose et al., 1999				Dunes	MIS 5d, 3	
Tuccimei et al., 2000				Cave deposits	MIS 7a, 5	U-Th
Tuccimei et al., 2006				Cave deposits		
0Vesica et al., 2000				Cave deposits	MIS 5e, 5d	U-Th
Vicens, 2015				Marine beach deposits	MIS 5d	U-Th
del Valle et al., 2016			Eivissa	Dunes	MIS 5e	
del Valle et al., 2020a				Aeolian deposits	MIS 6, 5, 4	OSL
del Valle et al., 2021a			Es Freus	Aeolian and pedogenetic deposits	MISS 22-6	OSL
del Valle et al., 2021b			Formentera	Aeolian and alluvial deposits	MIS 16-2	OSL
del Valle et al., 2021c				Aeolian and pedogenetic deposits	MIS 6, 5C, 4, 4/3	OSL
Zazo and Goy, 1990			Andalucia	Marine deposits	MIS 5e, MIS 2	OSL
Goy et al., 2006			Alicante	Cladora corals and dunes	MIS 5e	U-Series
Mauz et al., 2012				Marine terrases	MIS 7, 5	U-Series and OSL
Andreucci et al., 2009		Italy	Sardinia	Prograding beach system	MIS 5e	OSL
Andreucci et al., 2010a				Aeolian deposits	MIS 7,5	OSL
Pascucci et al., 2014				Dunes and alluvials	MIS 5.1, 5.3, 4	OSL
Carobene, 2015			Liguria	*L. lithophaga*	MIS 6, 5d, 4/3, 1	
Pappalardo et al., 2013				Aeolian deposits	MIS 5e	
Ferranti et al., 2006			Tuscany	Beach deposits	MIS 5.2, 5.1	OSL
Mauz, 1999				Dunes	MIS 5e	U-Series
Amorosi et al., 2014			Toronto	Marine deposits (P. latus)	MIS 5.3	OSL
Marra et al., 2019			Rome	*Glycymeris*	MIS 5e	ESR
Cerrone et al., 2021			Calabira	Marine deposits	MIS 5a, 5c, 5e	U-Series
Boenzi et al., 1985			Plugia	Marine deposits (P. latus)	MIS 5e	
Cai Pra and Hearty, 1988				Marine deposits (Glycymeris)	MIS 5e	AAR
Mastronuzzi et al., 2007				Marine deposits (P. latus) and Caves flowstone	MIS 9.3, 5e, 5a	
Mastronuzzi and Sansò, 2002a				Marine deposits and terrestrial fauna	MIS 5e, 1	14C
Mastronuzzi and Sansò, 2002b				Marine deposits and aeolianites	MIS 7, 5	14C, U-Series
Donnici and Serandrei Barbero, 2004			Venice	Lagoons dep., marine	MIS 5e, 5c	Foraminifera analysis
Tosi et al., 2007b				Lagoons dep., marine	MIS 5e, 5c	Foraminifera analysis
Antonioli et al., 2006			Sicilia	Marine deposits (P. latus)	MIS 5e, 5a, 5c	
Dubau et al., 2008		France	Provence	Marine shells	MIS 5	U-Series
Gilli, 2018				*Cladocora cespitosa*	MIS 5e	U-Series
Petit and Baley, 2000		United Kingdom	Gibraltar	Sand in a cave sequence	MIS 5.4, 5.3, 3	OSL
Rhodes et al., 2000				Aeolian sands	MIS 3	ESR
Rodríguez-Vidal et al., 2013				Fossils dunes	MIS 3	
Authemayou et al., 2016		Algheria	Tipasa	Beach deposits	MIS 7, 5	
Meghraoui et al., 1996			Oran	Marine deposits (P. latus)	MIS 5e	
Brueckner, 1986		Spain	Tarragona,	Aeolian dep.	MIS 5.4, 4	TL, ESR
Poujol et al., 2014		Morocco	Alicante	Marine dep. (mollusks)	MIS 5e	
Elmejdoub et al., 2011	Central M.	North Africa	Tunissia	Bioturbated dunes	MIS 5.4, 5.1, 3	OSL
Nathan and Mauz, 2008				Aeolianites	MIS 5.3, 5.2, 4	OSL
Mauz et al., 2009				Coastal dunes and marine terrases	MIS 5	
Frenchen et al., 2001	Eastern	Israel	Israel	Aeolianites	MIS 4, 3	TL
Engelman et al., 2001	Mediterranean		Israel	Aeolianites	MIS 3	TL
Sivan and Porat, 2004			Israel	Aeolianites	MIS 5.3, 4, 3	OSL
Frenchen et al., 2004			Carmel	Aeolianites	MIS 5.2, 5.1, 4, 3	IRSL
Sivan et al., 1999			Israel	Aeolian dep.	MIS 6	
El-Asmar, 1994		Egypt	Alexandria	Aeolianites	MIS 5.4, 5.3, 5.2	U-Series

(*continued on next page*)

Table 3 (*continued*)

Reference	Region	Country	Site	Original description	Time	Dating
El-Asmar and Wood, 2000				Aeolianites	MIS 9, 7, 5e, 5d	OSL
Macklin et al., 2002		Grecia	Grecia	Alluvial dep.	MIS 5b/4	
Macklin et al., 2002		Libia	Libia	Alluvial dep.	MIS 6, 5d, 4/3	

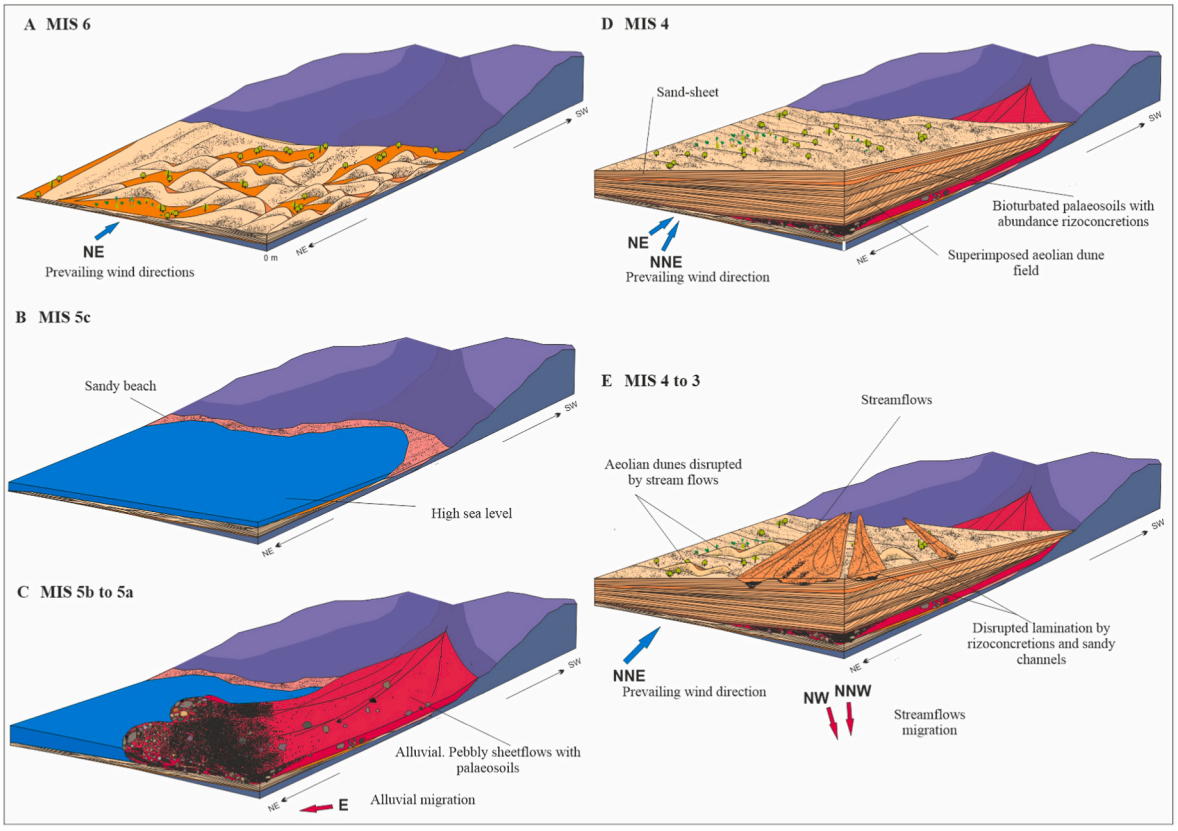

Fig. 7. Depositional environment evolution model showing the succession of the main sedimentary environments and paleocurrent directions of the Cala en Baster (Formentera) from MIS 6 to MIS 4/3.

ages 98 ± 8 ka (M#ES2# Es Copinar-Es Ram) and 91 ± 7 ka (M#IC2# Illa d'es Caragol) (Fig. 8 C and D). The decrease in sea level during the substage MIS 5b (Heinrich event 8 –H8-), favoured the formation of the dunes. These predominantly migrated from NE to SW entering inland through the most depressed areas. On the contrary during the following glacial sea level falling stage, concretely the transition of MIS 5b to the subtage MIS 5a alluvial - colluvial deposits developed on hillslopes and on the exposed shelf. The alluvial unit (i.e. Cala en Baster, M#CBP# 83 ± 7 ka) consists mainly of silty-matrix horizontal conglomerate beds and some palaeosoils on top with subangular clasts lenses (Figs. 7C and 8E). The absence of bioclastic material suggests that this is an alluvial unit and is indicative of a period of fan development. These structures indicate a paleocurrent to the East. Also, during the Pleistocene, the formation of palaeosoils in the western Mediterranean, as those described in U13, required warmer and relatively less arid conditions than the present conditions (**Potenciano et al., 1997**; **Wagner et al., 2014**; **Paskoff and Sanlaville, 1983**; **Mauz et al., 2013**). In this sense, **Rose et al. (1999)**; **Muhs et al. (2010)** and **Pomar et al. (2018)** had described important pedogenetic processes during the transition of MIS 5a to MIS 4 in the neighbouring island of Mallorca and the same kind of soils are present in the oriental Mediterranean coast of Israel (**Mauz et al., 2013**). In this way, in the middle of MIS 5a (H7b) and at the end of it (H7a), the cooling of the climate favoured the entrance of winds from the north. In this sense, in conditions of a relatively warmer sea temperature, episodes of strong storms developed with heavy rainfall that are caused erosion of the soils present on the slopes forming interdunar ponds. In addition, the dunes encroaching the coast and the base of this level were partially dismantled by the intense runoff and their sediment was deposited forming colluvial deposits with sandy channels.

Also, palaeosoils and reworked deposits are observed in Es Copinar-Es Ram, Cala Xuclar and Es Portitxol outcrops coinciding with the transition from MIS 5b to MIS 5a, which can also be observed at the U14 in the Pityusis Islands.

The transition between MIS 5 to MIS 4 (ca 75 ka) is marked by a rapid sea level fall (**Waelbroeck et al., 2002**; **Pascucci et al., 2014**; **Pomar et al., 2018**). During this period and the MIS 4 (H6) fully glacial conditions were established, with a sharp drop in sea level that again exposed the continental shelf and an extensive dune field formed (unit U15). According with the OSL data, the thick dune field present in Cala en Baster has an age of 72 ± 7 ka (M#CB3#), Illa des Penjats with an age of 87 ± 7 ka (#IP2#), Illa des Porcs with an age of 86 ± 7 ka (#IPC2#) and Illa des Caragol with an age of 84 ± 6 ka (M#IC1#) and Es Copinar-Es Ram with an age of 88 ± 8 ka (#ES7#) corresponding to this period (Figs. 7D and 8F). Similar deposits have been described in the northern part of Eivissa 73 ± 5 ka (M#D4# Cala Xuclar) (**del Valle et al., 2016**) as well as in Mallorca (**Fornós et al., 2009**) in Alicante

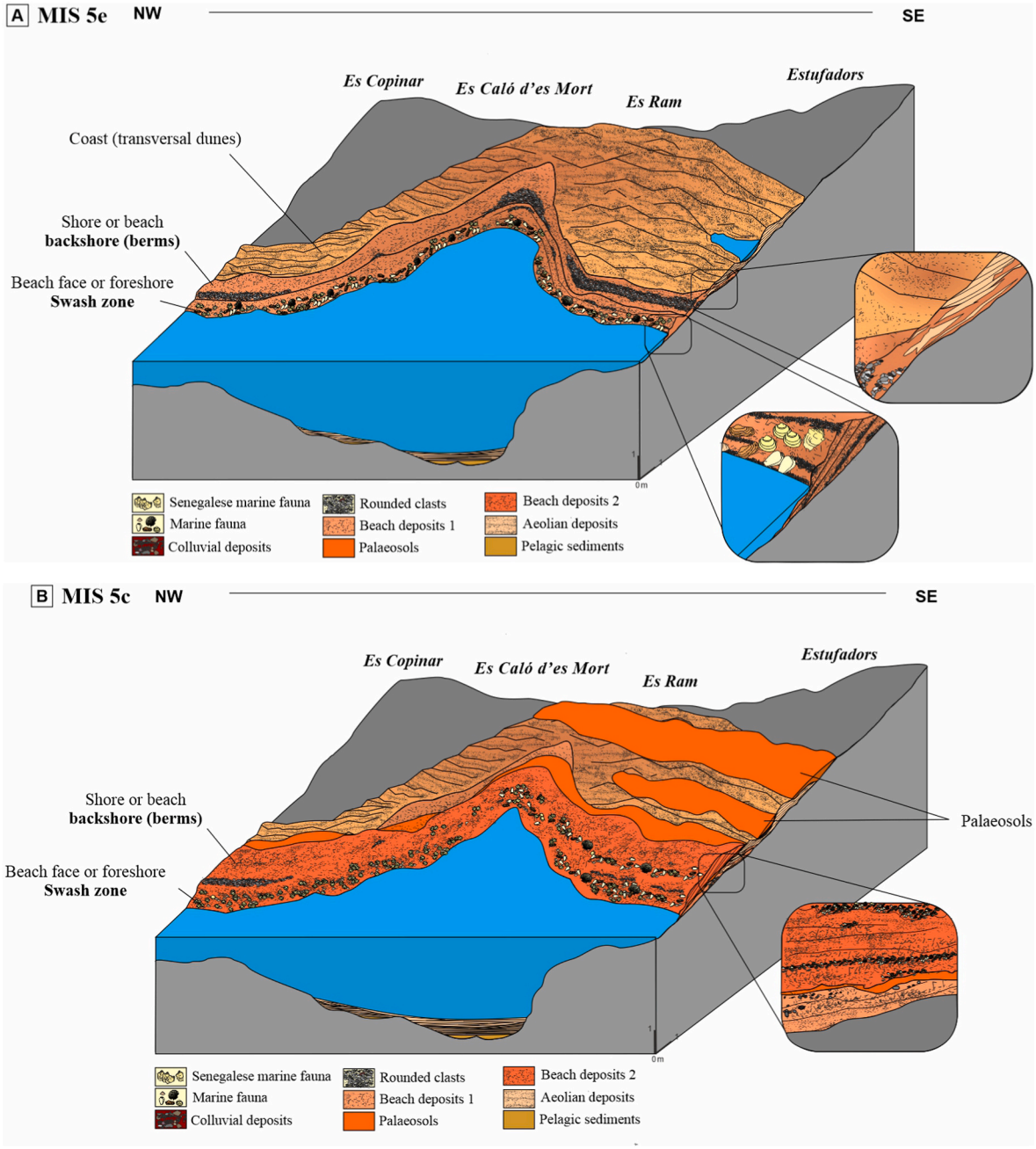

Fig. 8. Depositional environment evolution model showing the succession of the main sedimentary environments of the Es Ram- Es Copinar from MIS 5e to MIS 4.

(Brückner, 1986); Sardinia (Andreucci et al., 2009; Pascucci et al., 2014) and the oriental coast of the Mediterranean (Sivan and Porat, 2004; Frechen et al., 2001, 2004; Mauz et al., 2013; Nathan and Mauz, 2008).

Sandsheets, palaeosoil levels, and colluvial deposits are observed over the thick dune fields in Cala Xuclar, Cala en Baster, and Es Copinar-Es Ram. In other words, dry deposits with wind activity alternate with periods of more humid conditions with water influx, during which the aeolian dunes coexisted with palaeosoils or lacustrine levels at the end of the MIS 4 to MIS 3 (U16) (Fig. 7E). The muddy interdunar deposits (interdunar ponds) observed in Es Copinar-Es Ram indicate that the water table in interdune areas was so shallow. The OSL data (53.1 ± 5 ka Bardají et al., 2017) supports the attribution to this period.

The next unit U17 is composed of sandy channels, interpreted as streamflow. Additionally, the architecture of the unit, with abundant migrating channels, bars, erosive contacts or a complex lateral variability, indicates that this kind of features correspond to an alluvial environment. The sand grains composing sheet-flood deposits are rather similar to the aeolian ones (bioclastic) suggesting a reworking of dune sediments during ephemeral stream events and suggests that former aeolian sands were reworked prior to lithification or during a very early stage of lithification. Gibbling (2006) indicates that a combination of high magnitude water flows and high sediment availability may generate both deeply incised channels and infillings. The OSL ages of this unit (#CB4#- 70 ± 6 ka and #CB5#- 67 ± 5 ka) suggest that it was formed during the transition from MIS 4 to MIS 3. Based on the available data, we propose that the development of coastal alluvial fan in Cala en Baster and Cala Savina resulted from the combination of factors, including a drop-in sea level that generated enough space on the coast to expose the marine sediment and blow inland the sediment (forming the

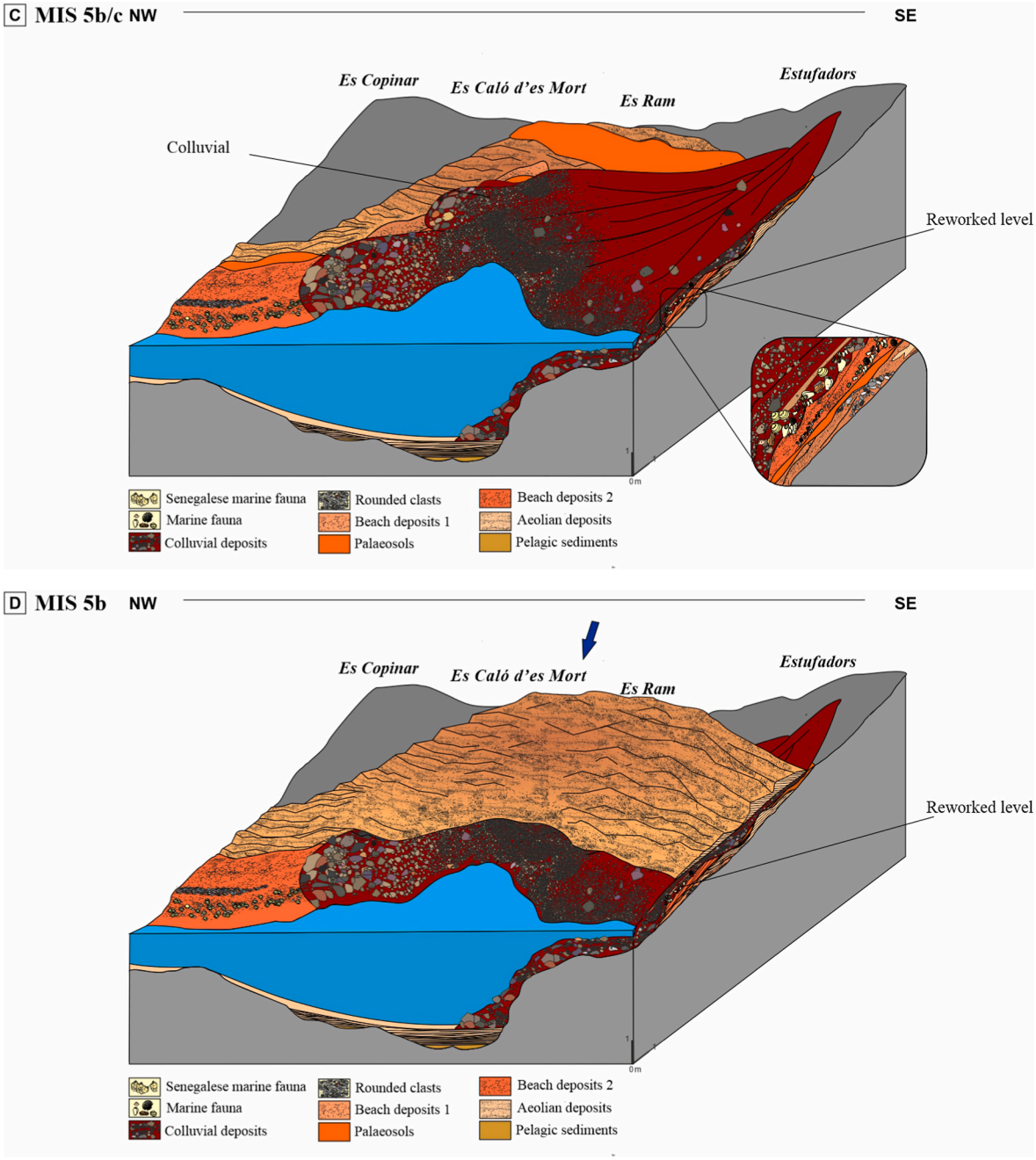

Fig. 8. (*continued*).

dune field). Additionally, a cooling climate context likely triggered temperature contrasts in the atmosphere, leading to episodes of intense rainfall. Furthermore, deposits with the same characteristics and chronology have already been made know in the north part of Eivissa (del Valle et al., 2016) and Mallorca, were Rose and Meng. (1999) and Pomar et al. (2018) have suggested an alluviation phase for northern Mallorca at the transition from MIS 4 to MIS 3.

During the middle of MIS 3, approximately 47.7 ± 3 ka, another period of dune formation occurred, coinciding with a sustained low sea level (Sidall et al., 2003; Rabineau et al., 2006). The next recorded wind activity episode is identified towards the end of MIS 3 around 39.8 ± 1 ka. The transition from MIS 3 to MIS 2 is characterized by the formation of a colluvial deposit, which can be attributed to changing atmospheric conditions during the last ice age. This period witnessed alternating fluctuations of relatively warm and cold climates occurring over a span of a few thousand years (Bond et al., 1999; Weaver et al., 1999; Schultz, 2002; Genty et al., 2003; Rahmstorf, 2003; Hemming, 2004; Martrat et al., 2004, 2007; Braun et al., 2005; Sprovieri et al., 2012; Incarbona et al., 2013; Long and Stoy, 2013; Rabassa and Ponce, 2013).The availability of sediment in Es Copinar-Es Ram outcrops resulted in the formation of deeply incised channels and subsequent infillings. These episodes were followed by a stable period characterized by soil formation, which were subsequently eroded and deposited as colluvial deposits during a warm episode MIS 3 and between H2 and H1. OSL data from Bardají et al. (2017) indicate the formation of a dune field during H1, approximately 18.8 ± 1.2, 16.1 ± 1.1 and 14.4 ± 1.2 ka, coinciding with MIS 2, when parts of the exposed platform were subjected to glacial conditions (Unit U19). Furthermore, OSL data of 18 ± 1 ka from the Illa des Porcs (#IPC3#) reveal the presence of palaeosoils or damp interdunar deposits in the Illa des Porcs

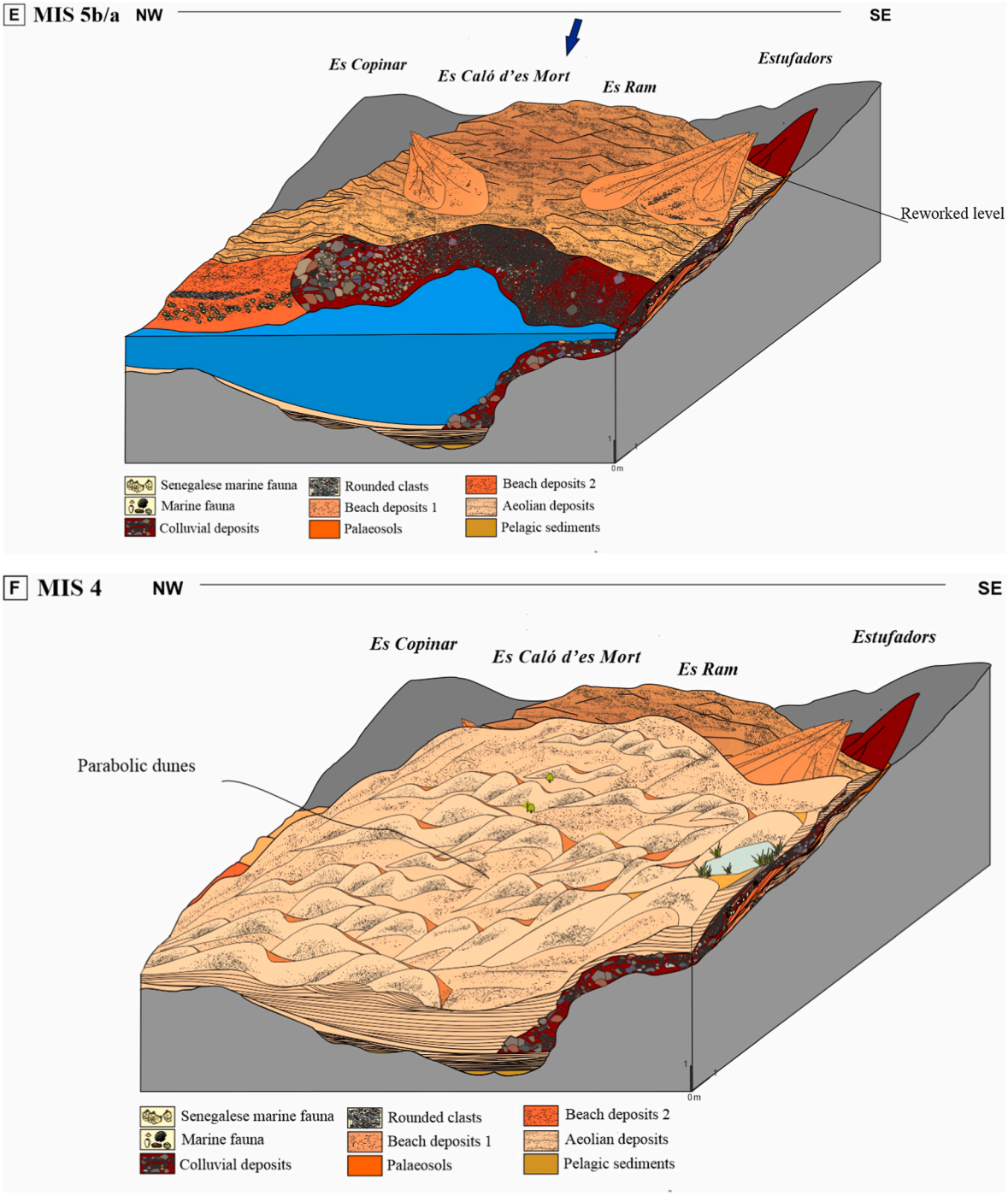

Fig. 8. (*continued*).

and S'Espalmador, indicating an stable period.

According to the data previously exposed, it is believed that there is a climatic correlation between the western and eastern coasts of the Mediterranean, coinciding both sedimentological and chronologically. Nonetheless, this correlation coincides with various places in the world, Morocco (Rhodes et al., 2006; El Kadiri et al., 2010); Bahamas (Carew and Mylroie, 2008) or Mexico (Ward, 1997) indicating continuous and diverse climatic fluctuations during the Quaternary.

6. Conclusions

The dated Pleistocene successions, characterized by the interference of aeolian, colluvial, alluvial, and marine deposits, as well as the intercalated pedogenetic deposits of the Pityusic islands, are instrumental archives for studying the influence of glacioeustatic sea level variation on coastal landscape evolution in the Mediterranean basin. These successions were correlated to temporal variations in climatic conditions that led to considerable changes in the sea level, and hence, in the accommodation space, as well as the supply of sands susceptible to aeolian mobilization.

We have obtained a better understanding of the interaction between sea level and climate based on the integration of the sedimentological and geomorphological studies, facies analysis, and associations of aeolian dunes, colluvial and marine deposits, coupled with optically

stimulated luminescence dating of the Pleistocene deposits of Pityusic Islands.

The analysis of the spatial distribution of the deposits and the erosion surfaces or contacts resulted in the identification of at least fourteen periods of aeolian accumulation of marine-source sediments. The abundance of bioclastic material on the coastal area during the interglacial periods, when the sea level was high, explains the origin of the sediments. The drop in the sea level and exposure of the large amount of marine sediments on the platform or exposed shelf areas resulted in accommodation space, leading to the development of dunes. Therefore, it is concluded that arid and cold stages (glacial stages) are represented by the development of the dune system.

The construction of the dune system exhibited a continuous sequence characterized by the successive development of superimposed dunes. This progression signifies in sediment availability over time. In addition, the morphology of the dunes is closely linked in size and complexity to the available accommodation space. Inland space and the rugged coastal terrain were secondary constraints on dune morphology and formation.

On the contrary, the formation of colluvial deposits, as well as the formation of soils, local episodes of ponds or arroyo like floodings, seems to be related to wetter conditions during interglacial stages. Additionally, the reddish colour of the edaphic levels, indicating a rubefaction process. Conversely, the presence of sandy palaeosoils suggests their formation occurred in a semi-arid environment, a notion supported by the abundant presence of bioclastic materials (sands) within them.

Optically stimulated luminescence (OSL) dating of the Pityusic deposits provided ages ranging from MIS 22 to MIS 2, and the obtained chronology reinforced the theory that episodes of aeolian activity took place during periods when the sea level was lower. The oldest units are located on the western coasts of the Pityusic Islands, and their OSL ages are consistent with the timing of the MIS 22.

The Middle Pleistocene deposits are located on the northern coast of Eivissa (e.g., Cala Xuclar, del Valle et al., 2016), the western coast of Eivissa, the southern coast of Eivissa, and the western part of the Espalmador islet. These sequences consist of approximately nine aeolian phases (where parabolic dunes and sand-sheet prevailed) interrupted by colluvial and pedogenetic deposits, showing the alternation of warm and humid moments, with cold and arid periods represented by the dunes. The OSL chronology provided ages consistent with the timing of the MIS 18 to MIS 6.

The youngest units, characterized by an extensive dune field composed mainly by parabolic dunes, are localized in Cala en Baster (Formentera), Cala Xuclar (Eivissa), Ses Salines (Eivissa) and the Es Freus Islets.

This dune field underwent erosive periods characterized by flashy water influxes leading to intense reworking of the aeolian dunes and sand-sheets, with the reworked bioclastic sand becoming part of the alluvial/colluvial environment. We propose that the observed interaction can due attributed to the transitional phases between glacial periods (MIS 4) and interglacial periods (MIS3) in the Late Pleistocene. Specifically, during the MIS 4/3 transition, significant thermal contrasts triggered episodes of intense precipitation, resulting in stream-flows or flash floods capable of causing partial or complete disintegration of the dune formations.

Periods of partial dune destruction, especially during the Late Pleistocene, are also linked to a decrease in sand availability, the formation of scour surfaces associated to an environmental change from arid to humid, with storms causing flash floods.

On the other hand, the beach deposits observed in s'Espalmador and Es Ram-Es Copinar indicate a sea level nearly 1 m above the current sea level, and the presence of Senegalese fauna certifies that this level corresponds to the MIS 5e. In this sense, the other beach deposits observed in Cala Xuclar (del Valle et al., 2016), in s'Espalmador islet, Cala en Baster (del Valle et al., 2020c) and the second beach level present in Es Ram-Es Copinar indicate an ancient sea level one to 3 m approximately above the current sea level. This marine level is related lithologically, stratigraphically, and faunistically to the warm isotopic stages MIS 5c/a.

The prevailing wind direction analysis performed on aeolian deposits indicates that during the Lower Pleistocene, the prevailing wind direction was from South, Southwest and in the final of this period the prevailing wind change to the North, North-east, while during the Middle Pleistocene, the prevailing wind direction was North-North-West. However, during the Late Pleistocene, the prevailing wind direction was changed to North-East and South-West.

Given that the study areas are geographically separated by the sea, the remarkable observation of complete bedrock coverage by Pleistocene deposits in this region, the observation of these deposits underwater; and their sedimentary characteristics suggests their uninterruptedly continuity, extending beyond the exposed surface to submerged extensions. The age information obtained by OSL lead us to conclude that throughout the regressive phases of the sea level, the Pityusic Islands and the islets of Es Freus were connected by extensive dunes fields, mainly consisting of parabolic dunes, evolving in some cases into climbing dunes or eco dunes, depending on the morphology of the basement. During interglacials, these dune fields were disconnected, and the formation of colluvial, pedogenetic, and marine deposits predominated.

The numerical data obtained in this study reaffirms the hypothesis that the Pleistocene deposits serve as reliable indicators of past climate variations. Similar Pleistocene sedimentary sequences and a consistent relationship between aeolianites, colluvial, and marine deposits formation and sea level be identified along mid-latitudes coasts of the Balearic Islands and the Mediterranean coastlines, this correlation will have significant implications for future paleoclimatic research. Furthermore, these findings can be utilized as valuable input data for predicting marine dynamics in the frame of climatic change.

Author's contributions

Laura del Valle: Methodology, data curation, investigation, formal análisis, visualization, writing-original draft-review and editing. **Alida TJimar-Gabor**: conceptualization, methodology, writing-review and editing, supervisión. **Joan J. Fornós**: funding acquisition, investigation, writing-review and editing.

Declaration of competing interest

The authors declare that they have no known competing financial interests or personal relationships that could have appeared to influence the work reported in this paper.

Data availability

Data will be made available on request.

Acknowledgement

This work was supported by the research found project AEI-MICINN, PID2020-112720 GB-100 (Spanish Government).

References

Adamiec, G., Aitken, M.J., 1998. Dose-rate conversion factors: update. Ancient TL 16, 37–50.

Alouane, M., 2001. Les formations quarternaries du secteurs littoraux du Maroc septentrional (régions de Tanger et de Nador): Analyse morphostructurale, lithostratigraphique et sédimentologique. thèse 3ème cycle. Université Mohamed VAGDAL, p. 206. Rabat (Morocco).

Amorosi, A., Antonioli, F., Bertini, A., Marabini, S., Mastronuzzi, G., Montagna, P., Negri, A., Rossi, V., Scarponi, D., Taviani, M., Angeletti, L., Piva, A., Battista, G., 2014. The middle-upper Pleistocene fronte section (Taranto, Italy): an exceptionally preserved marine record of the last interglacial. Global Planet. Change 119, 23—28. https://doi.org/10.1016/j.gloplacha.2014.04.007.

Andreucci, S., Clemmensen, L.B., Murray, A., Pascucci, V., 2010b. Middle Late Pleistocene coastal deposits of Alghero, northwestern Sardinia (Italy): chronology and evolution. Quat. Int. 222, 3–16. https://doi.org/10.1016/j.
Andreucci, S., Clemmensen, L.B., Murray, A., Pascucci, V., 2010a. Middle Late Pleistocene coastal deposits of Alghero, northwestern Sardinia (Italy): chronology and evolution. Quaternary International 222, 3–16. https://doi.org/10.1016/j.
Andreucci, S., Panzeri, L., Martini, P., Maspero, F., Martini, M., Pascucci, V., 2014. Evolution and architecture of a west mediterranean upper Pleistocene to Holocene coastal apron-fan system. Sedimentology 61, 333–361.
Andreucci, S., Pascucci, V., Murray, A.S., Clemmensen, L.B., 2009. Late Pleistocene coastal evolution of san giovanni di Sinis, west Sardinia (Western Mediterranean). Sediment. Geol. 216, 104–116. https://doi.org/10.1016/j.sedgeo.2009.03.001Getrightsandcontent.
Anechitei-Deacu, V., Timar-Gabor, A., Constantin, D., Trandafir-Antohi, O., Del Valle, L., Fornós, J.J., Gómez-Pujol, L., Wintle, A., 2018. Assessing the maximum limito f SAR-OSL Dating using Quartz of different grain sizes. Geochronometria 1–14.
Antonioli, F., Ferranti, L., Lambeck, K., Kershaw, S., Verrubbi, V., Dai Pra, G., 2006. Late Pleistocene to Holocene record of changing uplift rates in southern Calabria and northeastern sicily (southern Italy, central mediterranean sea). Tectonophysics 422 (1–4), 23–40. https://doi.org/10.1016/j.tecto.2006.05.003.
Authemayou, C., Pedoja, K., Heddar, A., Molliex, S., Boudiaf, A., Ghaleb, B., Van Vliet, B., Delcaillau, B., Djellit, H., Yelles, K., Nexer, M., 2016. Coastal uplift west of Algiers (Algeria): pre- and post-Messinian sequences of marine terraces and rasas and their associated drainage pattern. Int. J. Earth Sci. (Geol Rundsch) 106, 19–41. https://doi.org/10.1007/s00531-016-1292-5.
Bajo, P., Drysdale, R.N., Woodhead, J.D., Hellstrom, J.C., Hodell, D., Ferretti, P., Voelker, A.H.L., Zanchetta, G., Rodrigues, T., Wolff, E., Tyler, J., Frisia, S., Spötl, C., Fallick, A.E., 2020. Persistent influence of obliquity on ice age terminations since the Middle Pleistocene transition. Science 367, 1235–1239. https://doi.org/10.1126/science.aaw1114.
Bardají, T., Cabrero, A., Roquero, E., Zazo, C., Lario, J., Dabrio, C.J., Goy, J.L., Machado, M.J., Mercier, N., Silva, P.G., Martínez-Graña, A., 2017. Climatic variability in western Mediterranean during the last glacial cycle (ca. 130 – 14 ky BP): evidences from an island setting (Formentera, Balearic Is., Spain). In: PAGES OSM 2017 5th Open Science Meeting.
Bardají, T., Goy, J.L., Zazo, C., Hillaire-Marcel, C., Dabrio, C.J., Cabero, A., Ghaleb, B., Silva, P.G., Lario, J., 2009. Sea level and climate changes during OIS 5e in the Western Mediterranean. Geomorphology 104, 22–37.
Bateman, M.D., Carr, A.S., Dunajko, A.C., Holmes, P.J., Roberts, D.L., McLaren, S.J., Bryant, R.G., Marker, M.E., Murray-Wallace, C.V., 2011. The evolution of coastal barrier systems: a case study of the Middle-late Pleistocene Wilderness barriers, South Africa. Quat. Sci. Rev. 30, 63–81. https://doi:10.1016/j.quascirev.2010.10.003.
Blay, C.T., Longman, M.W., 2001. Stratigraphy and sedimentology of Pleistocene and Holocene carbonate eolianites, Kaua'I, Hawai'I U.S.A. Sedimentary Geology. SEPM 71.
Boenzi, F., Caldara, M., Pennetta, L., 1985. La Trasgressione Tirreniana nei dintorni di Castellaneta (Taranto). Geol. Appl. Idrogeol. 20, 163–175.
Bond, G.C., Showers, W., Elliot, M., Evans, M., Lotti, R., Hajdas, I., Bonani, G., Johnson, S., 1999. The North Atlantic's 1–2 kyr climate rhythm: Relation to Heinrich events, Dansgaard/Oeschger cycles and the Little Ice Age. In: Clark, P.U., Webb, R.S., Keigwin, L.D. (Eds.), Mechanisms of Global Climate Change at Millennial Time Scales, Geophys. Monogr. Ser., vol. 112. AGU, Washington, D, pp. 35–58.
Braun, H., Christl, M., Rahmstorf, S., Ganopolski, A., Mangini, A., Kubatzi, C., Roth, K., Kromer, B., 2005. Possible solar origin of the 1,470 year glacial climate cycle demonstrated in a coupled model. Nature 438, 208–211. https://doi.org/10.1038/nature04121.
Brooke, B., 2001. The distribution of carbonate eolianite. Earth Sci. Rev. 55, 135–164.
Brückner, H., 1986. Stratigraphy, evolution and age of Quaternary marine terraces in Morocco and Spain. Z. Geomorph. N.F., Suppl.- Bd. 62, 83–101.
Butzer, K.W., Cuerda, J., 1962. Coastal stratigraphy of southern Mallorca and its implication for the Pleistocene chronology of the Mediterranean Sea. J. Geol. 70, 398–416.
Carew, J.L., Mylroie, J.E., 2008. Quaternary carbonate eolianites of the Bahamas: useful analogues for the interpretation of ancient rocks?. In: Abegg, F.E., Harris, P.M., Loope, D.B. (Eds.), Modern and Ancient Carbonate Eolianites, vol. 71. SEPM Special Publication, pp. 33–45.
Carobene, L., 2015. Marine notches and sea-cave bioerosional grooves in microtidal áreas: Examples from the Thyrrhenian and Ligurian costas- Italy. J. Coast Res. 31 (3), 536–556. https://doi.org/10.2112/JCOASTRES-D-14-00068.1.
Cawthra, H.C., Jacobs, Z., Compton, J.S., Fisher, E.C., Karkanas, P., 2018. Depositional and sea-level history from MIS 6 (Termination II) to MIS 3 on the southern continental shelf of South Africa. Quat. Sci. Rev. 181, 156–172. https://doi.org/10.1016/j.quascirev.2017.12.002.
Cerrone, C., Vacchi, M., Fontana, A., Rovere, A., 2021. Last Interglacial Sea level proxies in the western Mediterranean. Earth Syst. Sci. Data. https://doi.org/10.5281/zenodo.4497365.
Claes, H., Soete, J., Van Noten, K., El Desouky, H., Marques-Erthal, M., Vanhaecke, F., Özkul, M., Swennen, R., 2015. Sedimentology, three-dimensional geobody reconstruction and carbon dioxide origin of Pleistocene travertine deposits in the Ballik área (South-west Turkey). Sedimentology 62 (5), 1408–1445.
Clemmensen, L.B., Fornós, J.J., Rodríguez-Perea, A., 1997. Morphology and achitecture of a late-Pleistocene cliff-front dune, Mallorca, Western Mediterranean. Terra. Nova 9, 251–254.
Clemmensen, L.B., Lisborg, T., Fornós, J.J., Bromley, R.G., 2001. Cliff-front aeolian and colluvial deposits, Mallorca, Western Mediterranean: a record of climatic and environmental change during the last glacial period. Bull. Geol. Soc. Den. 48, 217–232.
Cuerda, J., 1989. Los tiempos Cuaternarios en Baleares. Conselleria de Cultura, Educació i Esports del Govern Balear. 2° edición, vol. 305. Palma.
Cunningham, A.C., Murray, A.S., Armitage, S., Autzen, M., 2018. High-precision natural dose rate estimates through beta counting. Radiat. Meas. 120, 209–214.
Dai Pra, G., Hearty, P.J., 1988. 1 livelli marini pleistocenici del Golfo di Taranto. Sintesi geocronostratigrafica e tettonica. Memorie della Sociera Geológica Italiana 41, 637–644.
del Valle, L., 2016. El registre sedimentarieòlic del Plistocè Litoral d'Eivissa. Tesi Doctoral. Universitat de les Illes Balears, p. 286.
del Valle, L., Fornós, J.J., Pomar, F., Pons, G.X., Timar-Gabor, A., 2020c. Aeolian-alluvial interactions at Formentera (Balearic Islands, Western Mediterranean): The late Pleistocene evolution of a coastal system. Quat. Int. 566–567, 271–283. https://doi.org/10.1016/j.quaint.2020.05.010.
del Valle, L., Gómez-Pujol, L., Fornós, J.J., Timar-Gabor, A., Anechitei-Deacu, V., Pomar, F., 2016. Middle to Late Pleistocene dunefields in rocky coast settings at Cala Xuclar (Eivissa, Western Mediterranean): Recognition, architecture and luminescence chronology. Quat. Int. 407, 4–13.
del Valle, L., Pomar, F., Fornós, J.J., Gelabert, B., Timar-Gabor, A., 2021b. Processes and evolution of the Pleistocene coastal sedimentary succession of Es Codolar (Southern Eivissa, Balearic Islands, Western Mediterranean): insights from soft-sediment deformation structures. Environ. Earth Sci. 80 (754), 1–18. https://doi.org/10.1007/s12665-021-09966-z.
del Valle, L., Pomar, F., Fornós, J.J., Gómez-Pujol, L., Timar-Gabor, A., 2020b. Lower to middle Pleistocene coastal dune fields formation in the western Mediterranean (Western Eivissa, Balearic archipelago): chronology and landscape evolution. Aeolian Research 45, 100595. https://doi.org/10.1016/j.aeolia.2020.100595.
del Valle, L., Timar-Gabor, A., Fornós, J.J., 2019. Geomorphological Processes and Environmental Interpretation at Espalmador islet (Western Mediterranean). J. Mar. Sci. Eng. 7 (144), 1–14. https://doi.org/10.3390/jmse7050144.
del Valle, L., Timar-Gabor, A., Fornós, J.J., Pons, G.X., 2020a. Lower to Upper Pleistocene Coastal Deposits from the SesSalines, Es Freus Islets and Cala Savina (Pityusic Islands, Western Mediterranean): Chronology and Evolution. J. Coast Res. 95, 448–452.
del Valle, L., Timar-Gabor, A., Pomar, F., Pons, G.X., Fornós, J.J., 2021a. Millennial-scale climate variability recorded in Late Pleistocene coastal deposits of Formentera Island (Balearic Archipelago, Western Mediterranean). Quat. Int. 617, 112–128. https://doi.org/10.1016/j.quaint.2021.06.030.
Díaz,J .A.,2009.G uíad el aG eologísd eG ranada. http://www.granadanatural.com/blog.php?codigob loga rticulo=63.
Donnici, S., Serandrei Barbero, R., 2004. Paleogeografia e cronologia dei sedimenti tardo-pleistocenici ed olodenici presenti nel sottosuolo di Valle Averto (laguna di Venezia, bacion meridionale). Lavori SOc. Ven. Scienze Naturali 29, 101–108.
Dorale, J.A., Onac, P.B., Fornós, J.J., Ginés, J., Ginés, A., Tuccimei, P., Peate, D.W., 2010. Sea-level Highstand 81,000 Years Ago in Mallorca. Science 327, 860–863.
Duller, G.A.T., 2003. Distinguishing quartz and feldspar in single grain luminescence measurements. Radiat. Meas. 37, 161–165.
Dumas, B., Guérèmy, P., Raffy, J., 2005. Evidence for sea-level oscillations by the «characteristic thickness» of marine deposits from raised terraces of Southern Calabria (Italy). Quat. Sci. Rev. 24, 2120–2136.
Dumitru, O., Polyak, V., Asmerom, Y., Onac, B.P., 2020. Last interglacial (Sensu lato, ~130 to 75 ka) sea-level history from cave deposits: a global standardized database. Earth Syst. Sci. Data. https://doi.org/10.5194/essed-2020-387.
Dumitru, O., Polyak, V., Asmerom, Y., Onac, B.P., 2021. Last interglacial sea-level history from speleothems: a global standardized database. Earth Syst. Sci. Data 13 (5), 2077–2094. https://doi.org/10.5194/essd-13-2077-2021.
El Kadiri, K., Sanz de Galdeano, C., Antonip Pedrera, A., Chalouan, A., Galindo-Zaldívar, J., Julià, R., Akil, M., Hlila, R., Ahmamou, M., 2010. Eustatic and tectonic controls on Quaternary Ras Leona marine terraces (Strait of Gibraltar, northern Morocco). Quat. Res. 74, 277–288. https://doi.org/10.1016/j.yqres.2010.06.008.
El-Asmar, H., 1994. Aeoloianite sedimentation along the northwestern coast of egipt: evidence for middle to late quaternary aridity. Quat. Sci. Rev. 13, 699–708.
El-Asmar, H.M., Wood, P., 2000. Quaternary shoreline development: the north-western coast of Egypt. Quat. Sci. Rev. 19, 1137–1149. https://doi.org/10.1016/S0277-3791(99)00097-9.
Federici, P.R., Pappalardo, M., 2006. Evidence of marine Isotope Stage 5.5 highstand in Liguria (Italy) and its tectonic significance. Quat. Int. 145 (146), 68–77. https://doi.org/10.1016/j.quaint.2005.07.003.
Ferranti, L., Antonioli, F., Mauz, B., Amorisi, A., Dai Para, G., Mastronuzzi, G., Monaco, C., Pappalardo, M., Radtke, U., Renda, P., Romano, P., Sansó, P., Verrubi, V., 2006. Markers of the Last Interglacial sea level highstand along the coast of Italy: tectonic implications. Quat. Int. 145 (146), 30–54.
Fiol, L.L., Fornós, J.J., Gelabert, B., Guijarro, G.A., 2005. Pluges de pols a Mallorca (Mediterrani Occidental): la seva aparició i paper en alguns processos geològics recents. Catena 63, 64–84.
Flügel, E., 2014. Microfacies of Carbonate Rocks. Analysis, Interpretation and Application. Springer, Berlin, p. 976.
Fornós, J.J., Ahr, W.M., 1997. Temperate carbonates on a modern, low-energy, isolated ramp: The Balearic platform, Spain. J. Sediment. Res. 67, 364–373.
Fornós, J.J., Clemmensen, L.B., Gómez-Pujol, L., Murray, A., 2009. Late Pleistocene carbonate aeolianites on Mallorca, Western Mediterranean: a luminescence chronology. Quat. Sci. Rev. 28, 2697–2709.
Fornós, J.J., Gómez-Pujol, L., Clemmensen, L.B., 2004. Facies architecture of interbedded aeolianites and alluvial fans deposits: the Late Pleistocene of Pollença Bay (Mallorca

Is., Western Mediterrananean). In: International Association of Sedimentology 23rd Meeting, p. 116. Coimbra (Portugal).
Fornós, J.J., Clemmensen, L.B., Gómez-Pujol, L., Ginés, A., Ginés, J., 2012. Pleistocene eolianites and low sea levels. Gines J., A., Ginés, J., Gómez-Pujol, L., ONac, B.P., Fornós, J.J. Mallorca: a Mediterranean Benchmark for Quaternary Studies. Mon. Soc. Hist. Nart. Balears 18, 163–220.
Frechen, M., Derman, B., Boenigk, W., Ronen, A., 2001. Luminescence chronology of aeolianites from the section at Givat Olga Coastal Plain of Israel. Quat. Sci. Rev. 20, 805–809.
Frechen, M., Neber, A., Tsatskin, A., Boenigk, W., Ronene, A., 2004. Chronology of Pleistocene sedimentary cycles in the Carmel coastal plain of Israel. Quat. Int. 121, 41–52. https://doi.org/10.1016/j.quaint.2004.01.022.
García de Domingo, A., Díaz de Neira, J.A., Gil-Gil, J., Cabra-Gil, P., 2009. Cartografía y Memoria del Mapa Geológico de España a escala 1:25.000 (Plan MAGNA, 2ª serie) de la Hoja 799 I (Santa Eulària des Riu). Servicio de Publicaciones del IGME, Madrid, p. 77. Col·lecció 2ª Sèrie.
Genty, D., Blamart, D., Ouahdi, R., Gilmour, M., Baker, A., Jouzel, J., Van-Exter, S., 2003. Precise dating of Dansgaard-Oeschger climate oscillations in western Europe from stalagmite data. Nature 421, 833–837. https://doi.org/10.1038/nature01391.
Gibbard, P.L., Hughes, P.D., 2021. Terrestrial stratigraphical division in the Quaternary and its correlation. J. Geol. Soc. 178 (2) https://doi.org/10.1144/jgs2020-134.
Gibbling, M.R., 2006. Width and Thickness of Fluvial Channel Bodies and Valley Fills in the Geological Record: A Literature Compilation and classification. J. Sediment. Res. 76, 731–770.
Ginés, J., Formós, J.J., Ginés, A., Gràcia, F., Delita-la, C., Taddeucci, A., Tuccimei, P., Vesica, P.L., 2001. Els espeleotemes freàtics de les coves litorals de Mallorca: canvis del nivel de la Mediterrània i paleoclima en el Pleistocè superior. In: Pons, G.X., Guijarro, J.A. (Eds.), El canvi climàtic: passat, present i futur. Palma de Mallorca, vol. 9. Monografies de la Societat d'Història Natural de les Balears, pp. 33–52.
Hansen, V., Murray, A., Buylaert, J.-P., Yeo, E.-Y., Thomsen, C., 2015. A new irradiated quartz for beta source calibration. Radiat. Meas. 81, 123–127.
Hearty, P.J., 1998. The geology of Eleuthera Island, Bahamas: a Rosetta Stone of Quaternary stratigraphy and sea level history. Quat. Sci. Rev. 17, 333–335.
Hearty, P.J., Neumann, A.C., 2001. Rapid sea level and climate change at the close of the last Interglaciation (MIS 5e): evidence from the Bahama Islands. Quat. Sci. Rev. 20 (18), 1881–1895. https://doi.org/10.1016/S0277-3791(01)00021-X.
Hearty, P.J., O'Leary, M.J., 2008. Carbonate aeolianites, quartz sands and Quaternary sea-level cycles, Western Australia: a chronostratigraphic approach. Quat. Geochronol. 3, 26–55. https://doi.org/10.1016/j.quageo.2007.10.001.
Hemming, S.R., 2004. Heinrich events: Massive late Pleistocene detritus layers of the North Atlantic and their global climate imprint. Rev. Geophys. 42 (1), RG1005. https://doi.org/10.1029/2003RG000128. Bibcode:2004RvGeo.42.1005H.
Huerta, P., Rodríguez-Berriguete, A., Martín-García, R., Martín-Perez, A., La Iglesia Fernández, A., Alonso-Zarza, A.M., 2015. The role of climate and aeolian dust input in calcrete formation in volcanic islands (Lanzarote and Fuerteventura, Spain). Palaeogeogr. Palaeoclimatol. Palaeoecol. 417, 66–79.
Incarbona, A., Sprovieri, M., Di Stefano, A., Di Stefano, E., Salvagio, D., Pelosi, N., Ribera, M., Sprovieri, R., Ziveri, P., 2013. Productivity modes in the Mediterranean Sea during Dansgaard-Oeschger (20,000-70,000 yr ago) oscillations. Palaeogeogr. Palaeoclimatol. Palaeoecol. 392, 128–137. https://doi.org/10.1016/j.palaeo.2013.09.023.
Jacobs, Z., Roberts, D.L., 2009. Last Interglacial Age for aeolian and marine deposits and the Nahoon fossil human footprints, Southeast Coast of South Africa. Quat. Geochronol. 4 (2), 160–169. https://doi.org/10.1016/j.quageo.2008.09.002.
Jedoui, E., Davaud, H., Ismaïl, B., Reyss, J.L., 2002. Analyse sédimentologique des d'epôts marins pléistocènes du Sud-Est tunisien: mise en évidence de deux périodes de haut niveau marin pendant le sous-stade isotopique marin 5e (Eémien, Tyrrhénien). Bulletin Société Géologique du France 173, 63–72.
Just, J., Hübscher, C., Betzler, C., Lüdmann, T., Reicherter, K., 2011. Erosion of continental margins in the Western Mediterranean due to sea-level stagnancy during the Messinian salinity crisis. Geo Mar. Lett. 31, 51–64.
Kaspar, F., Spangehl, T., Cubasch, U., 2007. Northern Hemisphere winter storm tracks of the Eemian interglacial and the last glacial inception. Clim. Past 3, 181–192.
Kindler, P., Davaud, E., Strasser, A., 1997. Tyrrhenian coastal deposits from Sardinia (Italy): a petrographic record of high sea levels and shifting climate belts during the last interglacial (isotopic substage 5e). Palaeogeogr. Palaeoclimatol. Palaeoecol. 133, 1–25.
Kindler, P., Hearty, P.J., 1995. Pre-Sangamonian eolianites in the Bahamas? New evidence from Eleuthera island. Mar. Geol. 127, 73–86.
Kindler, P., Hearty, P.J., 1996. Carbonate petrology as an indicator of climate and sea level changes: new data from Bahamian Quaternary units. Sedimentology 43 (2), 381–399.
Klappa, C.F., 1980. Rhizoliths in terrestrial carbonates: classification, recognition, genesis and significance. Sedimentology 27, 613–629.
Kocurek, G., 1998. Response of the wind system to forcing external factors: a stratigraphic view of the Saharan region. In: Alsharhan, A., Glennie, K., Whittle, G., Kendall, C. (Eds.), Quaternary Deserts and Climate Change. Balkema, Rotterdam, pp. 327–337.
Lapp, T., Kook, M., Murray, A.S., Thomsen, K., Buylaert, J.P., Jain, M., 2015. A new Luminescence Detection and Stimulation Head for the Risø TL/OSL reader. Radiat. Meas. 81, 178–184.
Long, J.A., Stoy, P.C., 2013. Quantifying the periodicity of Heinrich and Dansgaard-Oeschger events during the Marine Oxygen Isotope Stage 3. Quat. Res. 79, 413–423.
Lowe, J.J., Walker, M.J.C., 2015. Reconstructing Quaternary Environments. Routledge, p. 538.
Macklin, M.G., Fuller, I.C., Lewin, J., Maas, G.S., Passmore, D.G., Rose, J., Woodward, J. C., Black, S., Hamnli, R.H.B., Rowan, J.S., 2002. Correlation of fluvial sequences in the Mediterranean basin over the last 200 ka and their relationship to climate change. Quat. Sci. Rev. 21, 1633–1641.
Martrat, B., Grimalt, J.O., Lopez-Martinez, C., Cacho, I., Sierro, F.J., Flores, J.A., Zahn, R., Canals, M., Curtis, J.H., Hodell, D.A., 2004. Abrupt temperature changes in the western Mediterranean over the past 250,000 years. Science 306, 1762–1765.
Martrat, B., Grimalt, J.O., Shackleton, N.J., de Abreu, L., Hutterli, M.A., Stocker, T.F., 2007. Four climate cycles of recurring deep and surface water destabilizations on the Iberian margin. Science 317, 502–507.
Mastronuzzi, G., Quinif, Y., Sansó, P., Selleri, G., 2007. Middle-Late Pleistocene evolution of a stable coastal área (southern Apulia, Italy). Geomorphology 86, 393–408. https://doi.org/10.1016/j.geomorph.2006.09.014.
Mastronuzzi, G., Sansò, P., 2002a. Holocene coastal dune development and environmental changes in Apulia (southern Italy). Sediment. Geol. 150 (1–2), 139–152. https://doi.org/10.1016/S0037-0738(01)00272-X. ISSN 0037-0738.
Mastronuzzi, G., Sansò, P., 2002b. Pleistocene sea-level changes, sapping processes and development of valley networks in the Apulia region (southern Italy). Geomorphology 46 (1–2), 19–34. https://doi.org/10.1016/S0169-555X(01)00172-6. ISSN 0169-555X.
Mauz, B., 1999. Late Pleistocene records of littoral processes at the Thyrrhenian Coast (Central Italy). Depositional environments and Luminsecence chronology. Quat. Sci. Rev. 18, 1173–1184. https://doi.org/10.1016/S0277-3791(98)00071-7.
Mauz, B., Fanelli, F., Elmejdoub, N., Barbieri, R., 2012. Coastal response to climate change: Mediterranean shorelines during the last interglacial (MIS 5). Quat. Sci. Rev. 56, 89–98. https://doi.org/10.1016/j.quascirev.2012.02.021.
Mauz, B., Hijma, M.P., Amorosi, A., Porat, N., Galili, E., Bloemendal, J., 2013. Aeolian beach ridges and their significance for climate and Sea Level. Concept and insight from the Levant Coast (East Mediterranean). Earth Sci. Rev. 121, 31–54. https://doi.org/10.1016/j.earscirev.2013.03.003.
Mauz, B., Sivan, D., Galili, E., 2020. MIS 5e Sea Level proxies in the eastern Mediterranean coast region Earth System Science Data. https://doi.org/10.5194/essd-2020-357.
Meghraoui, M., Morel, J.L., Andrieux, J., Dahmani, M., 1996. Tectonique plio-quaternaire de la chaine tello-rifaine et de la mer d'Alboran; une zone complexe de convergence ontinente-continent. Bull. Soc. Geol. Fr. 167 (1), 141–157.
Miall, A.D., 1996. The Geology of Fluvial Deposits. Sedimentary Facies, Basin Analysis, and Petroleum Geology. Springer, p. 582.
Miall, A.D., 2010. The Geology of Stratigraphic Sequences. Springer-Verlag. Berlin Heidelberg, p. 522, 2a Edició.
Moreno, A., Cacho, I., Canals, M., Prins, M.A., Sanchez-Goñi, M.F., Grimalt, J.O., Weltje, G.L., 2002. Saharan dust transport and high-latitude glacial climatic variability: the Alboran Sea record. Quat. Res. 58, 318–328.
Muhs, D.R., Budahn, J., Avila, A., Skipp, G., Freeman, J., Patternson, D., 2010. The role of African dust in the formation of Quaternary soils on Mallorca, Spain and implications for the genesis of Red Mediterranean soils. Quat. Sci. Rev. 29, 2518–2543.
Murray, A.S., Wintle, A.G., 2000. Luminescence dating of quartz using an improved single-aliquot regenerative-dose protocol. Radiat. Meas. 32, 57–73.
Murray, A.S., Wintle, A.G., 2003. The single aliquot regenerative dose protocol: potential for improvements in reliability. Radiat. Meas. 37, 377–381.
Muto, T., Steel, R.J., 2000. The accomodation concept in sequence stratigraphy: some dimensional problems and possible redefinition. Sediment. Geol. 130, 1–10.
Nathan, R.P., Mauz, B., 2008. On the dose-rate estimate of carbonate-rich sediments for trapped charge dating. Radiat. Meas. 43, 14–25.
Nielsen, K.A., Clemmensen, L.B., Fornós, J.J., 2004. Middle Pleistocene magnetostratigraphy and susceptibility stratigraphy: data from a carbonate aeolian system, Mallorca, Western Mediterranean. Quat. Sci. Rev. 23, 1733–1756.
Nolan, M.H., 1895. Rasgos generales de la estructura geológica del archipiélago balear. Bull. Soc. Geol. Fr. 23, 79–91.
Occhietti, S., Raynal, J.P., Pichet, P., Lefèvre, D., 2002. Aminostratigraphie des formations littorals Pléistocènes et holocènes de la region de Casablanca, Maroc. Quaternaire 13 (1), 55–64.
Pappalardo, M., Chelli, A., Ciampalini, A., Rellini, I., Biagroni, F., Brückner, H., Fülling, A., Firpo, M., 2013. Evolution of an Upper Pleistocene aeolianite in the northern Mediterranean (Ligura, NW, Italy). Italian J. Geosci. (Boll. Soc. Geol. It.). 132 (2), 290–303. https://doi.org/10.3301/IJG.2012.30.
Pascucci, V., Sechi, D., Andreucci, S., 2014. Middle Pleistocene to Holocene coastal evolution of NW Sardinia (mediterranean sea, Italy). Quat. Int. 328–329, 3–20.
Paskoff, R., Sanlaville, P., 1983. Les cˆotes de la Tunisie: Variations du Niveau Marin depuis le Tyrrhenien. Editions Maison de l'Orient, Lyon, France, p. 192.
Pavelic, D., Kovacic, M., Vlahovic, I., Wacha, L., 2011. Pleistocene calcareous aeolian-alluvial deposition in a steep relief karstic coastal belt (island of Hvar, eastern Adriatic, Croatia). Sediment. Geol. 239, 64–79.
Polyak, V.J., Onac, B.P., Fornós, J.J., Hay, C., Asmerom, Y., Dorale, J.A., Ginés, J., Tuccimei, P., Ginés, A., 2018. A highly resolved record of relative sea level in the western Mediterranean Sea during the last interglacial period. Nat. Geosci. 11, 860–864. https://doi.org/10.1038/s41561-018-0222-5.
Pomar, F., 2016. Arquitectura i fàcies deposicionals de la interferencia entre la sedimentació al·luvial, col·luvial i eólica a les Illes Balears durant el Pleistocè Superior: Implicacions Paleoclim'atiques. PhD. Universitat de les Illes Balears, p. 375.
Pomar, F., Del Valle, L., Fornós, J.J., Gómez-Pujol, L., 2015. Registro sedimentario litoral del Pleistoceno en las Islas Baleares (Mediterráneo occidental): implicaciones paleoclimáticas. VIII Jornadas deGeomorfología Litoral. Geotemas 15, 65–68.

Pomar, F., del Valle, L., Fornós, J.J., Gómez-Pujol, L., 2018. Late Pleistocene dune-sourced alluvial fans in coastal settings: Sedimentary facies and related processes (Mallorca, Western Mediterranean). Sediment. Geol. 367, 48–68.
Porat, N., Botha, G., 2008. The luminescence chronology of dune development on the Maputaland coastal plain, southeast Africa. Quat. Sci. Rev. 27 (9–10), 1024–1046.
Potenciano, A., Espejo, R., Garzón, G., 1997. Caracterización y ambiente de formación de los paleosuelos rojos en la cuenca terciaria del río Amarguillo (Toledo). Geogaceta 22, 157–160.
Poujol, A., Ritz, J.F., Tahayt, A., Vernant, P., Condomines, M., Blard, P.H., Billant, J., Vacher, L., Tibari, B., Hni, L., Koulali Idrissi, A., 2014. Active tectonics of the Northern Rif (Morocco) from geomorphic and geochronological data. J. Geodyn. 77, 70–88. https://doi.org/10.1016/j.jog.2014.01.004. ISSN 0264-3707.
Prescott, J.R., Hutton, J.T., 1994. Cosmic ray contributions to dose rates for luminescence and ESR dating: large depths and long terms variations. Radiat. Meas. 23 (2–3), 497–500.
Rabassa, J., Ponce, J.F., 2013. The Heinrich and Dansgaard-Oeschger climatic events during Marine Isotopic Stage 3: Searching for appropriate times for human colonization of the Americas. Quat. Int. 299, 94–105.
Rabineau, M., Berné, S., Olivet, J.L., Aslanian, D., Guillocheau, F., Joseph, P., 2006. Paleo sea levels reconsidered from direct observation of paleoshoreline position during Glacial Maxima (for the last 500,000 yr). Earth Planet Sci. Lett. 252, 119–137.
Rahmstorf, S., 2003. Timing of abrupt climate change: A precise clock. Geophys. Res. Lett. 30 (10).
Rhodes, E.J., Singarayer, J.S., Raynal, J.P., Westaway, K.E., Sbihi-Alaoui, F.Z., 2006. New age estimates for the Palaeolithic assemblages and Pleistocene succession of Casablanca, Morocco. Quat. Sci. Rev. 25, 2569–2585.
Roberts, E.M., Stevens, N.J., O'Connor, P.M., Dirks, P.H.G.M., Gottfried, M.D., Clyde, W. C., Armstrong, R.A., Kemp, A.I.S., Hemming, S., 2012. Initiation of the western branch of the East African Rift coeval with the eastern branch. Nat. Geosci. 5 (4), 289–294.
Rodrigues, T., Alonso-García, M., Hodell, D.A., Rufino, M., Naughton, F., Grimalt, J.O., Voelker, A.H.L., Abrantes, F., 2017. A 1-Ma record of sea surface temperature and extreme cooling events in the North Atlantic: A perspective from the Iberian Margin. Quat. Sci. Rev. 172, 118–130. https://doi.org/10.1016/j.quascirev.2017.07.004.
Rohling, E.J., Grant, K., Bolshaw, M., Roberts, A.P., Siddall, M., Hemleben, C., Kucera, M., 2009. Antarctic temperature and global sea level closely coupled over the past five glacial cycles. Nat. Geosci. 2, 500–504.
Rose, J., Meng, X., 1999. River activity in small catchments over the last 140ka, North-East Mallorca, Spain. In: Brown, A.G., Quine, T.A., Edrs (Eds.), Fluvial Processes and Environmental Change: 91-102. John Wiley & Sonso London.
Rose, J., Meng, X., Watson, C., 1999. Palaeoclimate and palaeoenvironmental responses in the western Mediterranean over the last 140 ka: evidence from Mallorca, Spain. J. Geol. Soc. 156, 435–448. https://doi.org/10.1144/gsjgs.156.2.0435 (London).
Sàbat, F., Gelabert, B., Rodríguez-Perea, A., Jiménez, J., 2011. Geological structure and evolution of Majorca: implications for the origin of the western Mediterranean. Tectonophysics 510, 217–238.
Schultz, M., 2002. On the 1470-years pacing of Dansgaard-Oescher warm events. Paleoceanography 17, 1–9.
Sessa, J.A., Callapez, P.M., Dinis, P.A., Hendy, A.J.W., 2013. Paleoenvironmental and paleobiogeographical implications of a middle Pleistocene mollusc assemblage from the marine terraces of Baia das Pipas, Southwest Angola. J. Paleontol. 87 (6), 1016–1040. https://doi.org/10.1666/12-119. D1016S03.00.
Shackleton, N.J., Vincent, E., 1978. Oxygen and carbon isotope studies in recent foraminifera from the southwest Indian Ocean. Mar. Micropaleontol. 3, 1–13.
Sidall, M., Rohling, E.J., Almogi-Labin, A., Hemleben, C.H., Melscher, D., Schmelzer, I., Smed, D.A., 2003. Sea-level fluctuations during the last glacial cycle. Nature 423, 853–858. https://doi.org/10.1038/nature001690.
Silva, P.G., Zazo, C., Bardají, T., Baena, J., Lario, J., Rosas, A., Van der Made, J., 2009. Tabla cronostratigràfica del Cuaternario de la Península Ibérica, v.2. AEQUA. Available at: www.aequa.es.
Sivan, D., Gvirtzman, G., Sass, E., 1999. Quaternary Stratigraphy and Paleogeography of the Galilee Coastal Plain, Israel. Quat. Res. 51, 280–294. https://doi.org/10.1006/qres.1999.2044.
Sivan, D., Porat, N., 2004. Evidence from luminescence for Late Pleistocene formation of calcareous aeolianite (kurkar) and paleosol (hamra) in the Carmel Coast, Israel. Palaeogeogr. Palaeoclimatol. Palaeoecol. 211, 95–106. https://doi.org/10.3301/IJG.2012.30.
Sprovieri, M., Di Stefano, E., Incarbona, A., Salvagio, M., Pelosi, N., Ribera d'Alcala, M., Sprovieri, R., 2012. Trace metal/Ca Ratios Measured on Globigerinoides Ruber Shells of Selected Intervals at ODP Site 160-963. PANGAEA. https://doi.org/10.1594/PANGAEA.815999 (Table 1) In supplement to: Sprovieri, M et al. (2012): Centennial- to millennial-scale climate oscillations in the Central-Eastern Mediterranean Sea between 20,000 and 70,000 years ago: evidence from a high-resolution geochemical and micropaleontological record. Quaternary Science Reviews, 46, 126-135.
Sun, J., Ding, Z., Liu, T., Rokosh, D., Rutler, N., 1999. 580.000-year environmental reconstruction from aeolian deposits at the Mu Us Desert Margin, China. Quat. Sci. Rev. 18, 1351–1364.
Toker, E., Kayseri-Özer, M.S., Özkul, M., Kele, S., 2015. Depositional system and palaeoclimatic interpretations of Middle to Late Pleistocene travertines: Kocabaş. Denizli, south-west Turkey 62 (5), 1360–1383.
Tosi, L., Rizzetto, F., Bonardi, M., Donnici, S., Serandrei Barbero, R., Toffoletto, F., 2007b. Note illustrative della Carta Geologica d'Italia alla scala 1:50.000, 148–149. Chioggia-Malamocco. APAT, Dipartimento Difesa del Suolo, Servizio Geologico d'Italia, Casa Editrice SystemCart, Roma, p. 164, 2 fogli.
Tuccimei, P., Ginés, J., Delitala, C., Pazzeli, L., Taddeucci, A., Clamor, B., Fornós, J.J., Ginés, A., Gràcia, F., 2000. Dataciones Th/U de espeleotemas freáticos recolectados a cotas inferiores al actual nivel marino en cuevas costeras de Mallorca (España): Aportaciones a la construcción de una curva eustática detallada de los últimos 300 ka para el Mediterráneo Occidental. Endins 23, 59–71.
Tuccimei, P., Ginés, J., Delitala, M.C., Gin_es, A., Gràcia, F., Fornós, J.J., Taddeucci, A., 2006. High precision U-series data from phreatic overgrowths on speleothems. Z. Geomorphol. 50 (1), 1–21.
Tucker, M.E., 1988. Techniques in Sedimentology. Blackwell Scientific Publications, pp. 355–386.
Vandenberghe, D.A.G., De Corte, F., Buylaert, J.-P., Kučera, J., Van den haute, P., 2008. On the internal radioactivity in quartz. Radiat. Meas. 43, 771–775.
Vesica, P.L., Tuccimei, P., Turi, B., Fornós, J.J., Ginés, A., Ginés, J., 2000. Late Pleistocene Paleoclimates and sea-level change in the Mediterranean as inferred from stable isotopes and U-series studies of overgrowths on speleothems. Quat. Sci. Rev. 19, 865–879.
Vicens, D., 2015. El registre paleontològic dels dipòsits litorals quaternaris a l'illa de Mallorca (Illes Balears, Mediterrània Occidental). Tesi doctoral. UIB, p. 1011.
Waelbroeck, C., Labeyrie, L., Michel, E., Duplessy, J.C., McManus, J.F., Lambeck, K., Balbon, E., Labracherie, M., 2002. Sea-level and deep-water temperature changes derived from benthonic foraminifera isotopic records. Quat. Sci. Rev. 21, 295–305.
Wagner, S., Eckmeier, E., Skowronek, A., Günster, N., 2014. Quaternary paleosols and sediments on the Balearic Islands as indicators of climate changes. Catena 112, 112–124.
Ward, W.C., 1997. Geology of coastal islands, north eastern Yucatan Peninsula. In: Vacher, H.L., Quinn, L. (Eds.), Geology and Hydrogeology of Carbonate Islands. Developments in Sedimentology, 54. Elservier Science B.V. Publishers, pp. 275–298.
Weaver, A.J., Bitz, C.M., Fanning, A.F., Holland, M.M., 1999. Thermohaline circulation: High-Latitude Phenomena and the Difference Between the Pacific and Atlantic. Annu. Rev. Earth Planet Sci. 27, 231–285.
WoRMS, 2020. World Register of Marine Species. http://www.marineespecies.org/index.php.
Zazo, C., 1999. Interglacial sea levels. Quat. Int. 55, 101–113.
Zazo, C., 2006. Cambio Climático y nivel del mar: La península Ibérica en el contexto Global. Revista Cuaternario y Geormorfología 20 (3–4), 115–130.